이학박사 학위논문

Generation of a nebulizable CDR-modified MERS-CoV neutralizing human antibody

상보성 결정 영역 돌연변이를 통한 분무 가능한 중동호흡기증후군 코로나바이러스 중화 인간 항체 개발

2020 년 2 월

서울대학교 대학원

의학과 협동과정 종양생물학전공

김 상 일

상보성 결정 영역 돌연변이를 통한 분무 가능한 중동호흡기증후군 코로나바이러스 중화 인간 항체 개발

지도 교수 정 준 호

이 논문을 이학박사 학위논문으로 제출함

2019년 10월

서울대학교 대학원

협동과정 종양생물학 전공

김 상 일

김상일의 이학박사 학위논문을 인준함

2020년 1월

위 원 장 _____ (인)

부위원장 _____ (인)

위 원 _____ (인)

위 원 _____ (인)

위 원 _____ (인)

A thesis of the Degree of Doctor of Philosophy

상보성 결정 영역 돌연변이를 통한 분무 가능한 중동호흡기증후군 코로나바이러스 중화 인간 항체 개발

Generation of a nebulizable CDR-modified MERS-CoV neutralizing human antibody

February 2020

The Department of cancer biology,

Seoul National University

College of Medicine

Sang Il Kim

Generation of a nebulizable CDR-modified MERS-CoV neutralizing human antibody

by

Sang Il Kim

A thesis submitted to the Department of cancer biology in partial fulfillment of the requirements for the Degree of Doctor of Philosophy in Cancer Biology at Seoul National University College of Medicine

January 2020

Approved by Thesis Committee:

Professor _____**Chairman**

Professor _____**Vice chairman**

Professor _____

Professor _____

Professor _____

Abstract

Middle East respiratory syndrome coronavirus (MERS-CoV) induces severe aggravating respiratory failure in infected patients, frequently resulting in mechanical ventilation. As limited therapeutic antibody is accumulated in lung tissue following systemic administration, inhalation is newly recognized as an alternative, possibly better, route of therapeutic antibody for pulmonary diseases. The nebulization process, however, generates diverse physiological stresses, and thus, the therapeutic antibody must be resistant to these stresses, remain stable, and form minimal aggregates. We first isolated a MERS-CoV neutralizing antibody that is reactive to the receptor-binding domain (RBD) of spike (S) glycoprotein. To increase stability, we introduced mutations into the complementarity-determining regions (CDRs) of the antibody. In the HCDRs (excluding HCDR3) in this clone, two hydrophobic residues were replaced with Glu, two residues were replaced with Asp, and four residues were replaced with positively charged amino acids. In LCDRs, only two Leu residues were replaced with Val. These modifications successfully generated a clone with significantly greater stability and equivalent reactivity and neutralizing activity following nebulization compared to the original clone. In summary, we generated a MERS-CoV neutralizing human antibody that is reactive to recombinant MERS-CoV S RBD protein for delivery via a pulmonary route by introducing stabilizing mutations into five CDRs.

Keyword : MERS-CoV; aerosol delivery; nebulizer; neutralizing antibody; antibody engineering, pulmonary disease, complementarity-determining regions

Student Number : 2014-25080

Contents

List of Tables

List of figures

Abbreviations

MERS-CoV:	Middle East respiratory syndrome coronavirus
DPP4:	dipeptidyl peptidase 4
RBD:	receptor-binding domain
i.v.:	intravenous
mAb:	monoclonal antibody
CDR:	complementarity-determining region
scFv:	single-chain variable fragment
PBMC:	peripheral blood mononuclear cell
SE-HPLC:	size-exclusion high-performance liquid chromatography
DLS:	dynamic light scattering
PRNT:	plaque reduction neutralization test
HDX-MS:	Hydrogen/deuterium exchange mass spectrometry

Purpose of the study

Infectious diseases are the leading cause of death worldwide; sudden emergences and the possibility of re-emergences of infectious diseases such as MERS-CoV underscore the importance of establishing proper systems and procedures that support ongoing research and thereby allow us to be prepared with robust countermeasures and effective treatments. Despite increased awareness of such threats to the global public health and resilient efforts throughout the scientific and medical communities, no vaccine or antiviral agent for MERS-CoV is currently available. MERS-CoV induces severe respiratory failure in infected patients that frequently results in mechanical ventilation. Traditional systemic administration limits accumulation of therapeutic antibodies in lung tissue, and thus inhalation may be a more effective alternative delivery route for therapeutic antibodies to treat pulmonary diseases. As support for our hypothesis, we sought to generate a MERS-CoV neutralizing antibody for delivery via a pulmonary route by introducing stabilizing mutations into CDRs.

1. Introduction

Middle East respiratory syndrome coronavirus (MERS-CoV) was first identified in Saudi Arabia in 2012 from a patient who suffered acute pneumonia and subsequent renal failure [1]. Since then, the World Health Organization has reported 2254 laboratory-confirmed cases of MERS-CoV infections in 27 different countries around the world, and South Korea has recorded the highest number of cases outside of the Middle East. Despite resilient efforts throughout the scientific and medical communities, no vaccine or antiviral agent for MERS-CoV is currently available.

MERS-CoV is a large (30 kb), enveloped, single-stranded, positive-sense RNA virus. The viral genome encodes four major structural proteins: spike (S), envelope (E), membrane (M), and nucleocapsid (N) proteins [2]. The S glycoprotein is a major envelope protein and interacts with the cellular receptor dipeptidyl peptidase 4 (DPP4) for entry into the host cell [3]. This protein consists of the S1 and S2 subunits. The receptor-binding domain (RBD) within the S1 subunit mediates receptor binding, whereas the S2 subunit facilitates membrane fusion. DPP4 is expressed on a variety of human cells, including fibroblasts, intestinal epithelial cells, and hepatocytes [4], as well as in the lung parenchyma and interstitium [5,6]. MERS-CoV is detected in respiratory secretions and the lower respiratory tract of the infected patients [7,8]. In the most severe cases of MERS-CoV infection, aggravating respiratory failure ultimately results in mechanical ventilation [9]. These observations suggest that the MERS-CoV virus primarily infects the human respiratory tract and replicates within the human airway epithelium [10,11].

Antibodies play a crucial role in the prevention and treatment of viral infection. Polysera taken from recovered patients and vaccinated donors have been used as prophylactic agents for hepatitis B, rabies, and other viral diseases [12–14]. Palivizumab (Synagis, Medimmune, Gaithersburg, MD, USA) was approved for the prophylaxis of RSV in 1998, and ibalizumab-uiyk (Trogarzo, TailMed Biologics, Taiwan) became clinically available in 2018 for the treatment of human immunodeficiency virus type 1 (HIV-1) infection in treatment-experienced adults with multi-drug-resistant HIV-1 and failure to respond to the current antiretroviral regimen.

In response to the ongoing epidemic, several groups have developed anti-MERS-CoV neutralizing monoclonal or polyclonal antibodies that target RBD [15,16]. These antibodies were generated from B cells derived from convalescent patients, nonimmune human antibody phage-display libraries, fully humanized mice, transchromosomic bovines, or hybridomas from mice that were immunized with MERS-CoV S. These antibodies potently inhibit RBD binding to the DPP4 receptor [17–23]. Furthermore, therapeutic effects of RBD-specific neutralizing antibodies were evaluated in several animal models, including Ad5/hDPP4-trasduced mice, humanized DPP4 mice, and hDPP4-transgenic mice as well as hDPP4-knock-in mice, rabbits, and rhesus monkeys [17,21,24–30].

All MERS-CoV neutralizing antibodies were developed for intravenous (i.v.) delivery; however, recent reports indicate that the amount of antibody delivered to lung tissue is often quite limited following systemic delivery [31,32]. In cynomolgus monkeys, bronchoalveolar lavage fluid contained dose-proportional concentrations of systemically administrated antibody, and these concentrations were

approximately 500-fold less than those in plasma [31]. Therefore, delivery of therapeutic antibody to lung tissues via inhalation has garnered considerable interest. Following delivery via the airway, cetuximab, an anti-epidermal growth factor receptor (EGFR) antibody, accumulated in normal and cancerous tissues in the lung at a concentration that was twice that achieved after i.v. delivery [33]. In addition, recent studies showed that Fc fusion proteins and nanobodies are also efficiently delivered via the pulmonary route [34–37]. Therefore, MERS-CoV neutralizing antibody may also accumulate at higher concentrations following delivery via a pulmonary route, suggesting higher efficacy. In order for this pulmonary delivery to be successful, the antibody must be sufficiently stable to resist denaturation during the process of nebulization.

In this study, we generated a MERS-CoV neutralizing antibody for delivery via nebulization. We constructed a phage-display library from two convalescent MERS-CoV-infected patients and successfully isolated nine MERS-CoV RBD-specific neutralizing mAbs. After nebulization, these antibodies showed significant aggregation and reduced reactivity to recombinant S glycoprotein. We therefore reduced the number of hydrophobic residues and introduced solubilizing mutations within the complementarity-determining regions (CDRs), generating an antibody that is resistant to aggregation during nebulization and retains its MERS-CoV neutralizing activity.

2. Materials and Methods

2.1. Ethics Statement

The study that provided the human samples was approved by the Institutional Ethics Review Board of Seoul National University Hospital (IRB approval number: 1602-100-742), and written informed consent was obtained from all participants.

2.2. Construction of A Human scFv Phage-Display Library and Three Randomization Libraries

PBMCs were isolated from two MERS-CoV-infected convalescent patients using a Ficoll-Paque density gradient medium (GE Healthcare, Pittsburgh, PA, USA) as described previously [63]. The PBMCs were subjected to total RNA isolation using the TRI Reagent (Invitrogen, Carlsbad, CA, USA) following the manufacturer's instructions. The RNA was used to synthesize cDNA using Superscript III First-Strand Synthesis system (Invitrogen) with oligo(dT) primers according to the manufacturer's instructions. Using the cDNA as a template, the genes encoding the variable regions of heavy and light chains (V_H and V_K/V_λ) were amplified and used for the construction of a human scFv phage-display libraries as described previously [64,65].

For the construction of the first randomization library, a set of degenerate Ultramer DNA oligonucleotides (Integrated DNA Technologies, Coralville, IA, USA) encoding residues from H1 to H65 of clone C-8 (V_{HN1}) was chemically synthesized to contain either a codon encoding the wild-type amino acid or a GAK degenerate codon at the H29, H32, H51, H52, H53, and H54 residues (Table 2). Then, the gene fragment (V_{HC}) encoding residues from H58 to H113 of clone C-8 was amplified by PCR using primer set 1 (Table 1) in a T100 Thermal Cycler (Bio-Rad, Carlsbad, CA, USA). The PCR conditions were as follows: preliminary denaturation at 94 ℃ for 5 min, followed by 25 cycles of 15 s at 94 ℃, 15 s at 56 ℃ and 90 s at 72 ℃. A final extension was then conducted for 10 min at 72 ℃. After electrophoresis on a 1% agarose gel, the PCR products were purified using QIAquick gel extraction kit (Qiagen Inc., Valencia, CA, USA) according to the manufacturer's instructions. The purified V_{HN1} and V_{HC} gene fragments were mixed at a concentration of 100 ng and subjected to linker PCR using primer set 2 (Table 1) in a T100 Thermal Cycler to yield the V_{H1} fragment. The PCR conditions were as follows: preliminary denaturation at 94 ℃ for 5 min, followed by 25 cycles of 15 s at 94 ℃, 15 s at 56 ℃ and 120 s at 72 ℃. The reaction was ended with an extension step for 10 min at 72 ℃. The gene fragment encoding V_L (V_{L1}) of clone C-8 was amplified by PCR using primer set 3 (Table 1) with the same PCR conditions described above for amplification of V_{HC}. Then, the V_{H1} and V_{L1} fragments were subjected to electrophoresis on a 1% agarose gel, and excised bands were purified using the QIAquick gel extraction kit. The purified V_{H1} and V_{L1} fragments were used for the synthesis of the scFv gene ($scFv_1$) using PCR as described previously [64]. The

amplified $scFv_1$ fragment was purified and cloned into the phagemid vector as described [64,65].

For the construction of the second randomization library, a set of degenerate Ultramer DNA oligonucleotides encoding residues from H1 to H65 of clone C-8-2 (V_{HN2}) was chemically synthesized to contain either a codon encoding the wild-type amino acid or a GAK degenerate codon at the H26 to H33 (HCDR1) and H51 to H57 (HCDR2) residues (Table 2), excluding the previously randomized residues. The V_{HN2} and V_{HC} gene fragments were mixed at equal ratios at 100 ng and subjected to linker PCR using primer set 2 (Table 1) in a T100 Thermal Cycler to yield the V_{H2} gene fragment as described above. The V_{H2} gene fragment was purified as described above and subjected to linker PCR with V_{L1} fragments to yield the $scFv_2$ gene fragment, which was cloned into the phagemid vector as described above.

For the construction of the third randomization library, two sets of degenerate Ultramer DNA oligonucleotides with a length of 200 nucleotides were chemically synthesized. One set encoded from L1 to L61 residues of clone C-8 (V_{LN}), while the other one encoded from L56 to L107 of clone C-8 (V_{LC}). These degenerate oligonucleotides contained either a codon encoding the wild-type amino acid or a GAK degenerate codon at L27B, L27C, L30, L32, L50, L89, L92, and L96 residues (Table 2). The V_{LN} and V_{LC} gene fragments (100 ng each) were subjected to a linker PCR using primer set 3 (Table 1) in a T100 Thermal Cycler to produce the VL_2 gene fragment using the same PCR conditions as described above for the amplification of the V_{H1} gene fragment. The gene fragment encoding V_H of C-8-2-4B (VH_3) was amplified by PCR using primer set 2 (Table 1) using the same PCR conditions used for the amplification of the V_{HC} gene fragment as described above. After purification,

VL_2 and VH_3 gene fragments were used to produce the $scFv_3$ gene fragment, which was cloned into the phagemid vector as described above.

Table 1. Primers used for the generation of the randomized libraries

Primer set 1	Forward: 5'-AACTACGCACAGAAGTTCCAGGGCAG-3' Reverse: 5'-GGCCGGCCTGGCCTGAGGAGACGGTGACCGTG-3'
Primer set 2	Forward: 5'-GTGGCTCGGGCGGTGGTGGGGAGGTGCAGCTGGTGCAGTCTGG -3' Reverse: 5'-GGCCGGCCTGGCCTGAGGAGACGGTGACCGTG-3'
Primer set 3	Forward: 5'-GGCCCAGGCGGCCGAGCTCGTGATGACTCAGTCTCCA-3' Reverse: 5'-CCCACCACCGCCCGAGCCACCGCCACCAGAGGAGGAAGATCTAGAGGAACCACCTTTGATTTCCACCTTGGTCCCTC-3'

Table 2. Degenerate codons used in the randomized libraries

The first library																	
	HCDR1									HCDR2							
Kabat number	H26	H27	H28	H29	H30	H31	H32	H33		H51	H52	H52A	H53	H54	H55	H56	H57
Amino acid	G	G	T	F	S	S	Y	A		I	I	P	F	F	G	T	A
Degenerate codon				KWK			KAK			RWK	RWK		KWK	KWK			
Amino acids encoded by the degenerate codon				D,E,F, LV,Y			D,E,Y			I,M,N, K,V,D, E	I,M,N, K,V,D, E		F,L,Y, V,D,E	F,L,Y, V,D,E			

The second library																
	HCDR1								HCDR2							
Kabat number	H26	H27	H28	H29	H30	H31	H32	H33	H51	H52	H52A	H53	H54	H55	H56	H57
Amino acid	G	G	T	E	S	S	E	A	I	I	P	F	F	G	T	A
Degenerate codon	GRK	GRK	RMK		RRK	RRK		GMK						GRK	RMK	GMK
Amino acids encoded by the degenerate codon	G,D,E	G,D,E	T,N,K, A,D,E		S,R,K,N ,G,D,E	S,R,K,N ,G,D,E		A,D,E						G,D, E	T,N, K,A, D,E	A,D,E

The third library																						
	LCDR1											LCDR2			LCDR3							
Kabat number	L27	L27A	L27B	L27C	L27D	L27E	L28	L29	L30	L31	L32	L50	L51	L52	L89	L90	L91	L92	L93	L94	L95	L96	L97
Amino acid	Q	S	L	L	H	S	N	G	Y	N	Y	L	G	S	M	Q	A	L	Q	T	P	L	T
Degenerate codon			SWK	SWK					KAK		KAK	SWK			RWK			SWK				SWK	
Amino acids encoded by the degenerate codon			L,F,H ,Q,V, D,E	L,F,H ,Q,V, D,E					Y,D,E		Y,D,E	L,F,H, Q,V,D ,E			M,I,K ,N,V, D,E			L,F,H ,Q,V, D,E				L,F,H ,Q,V, D,E	

2.3. Biopanning

The human scFv phage-display libraries were subjected to four rounds of biopanning against recombinant MERS-CoV S RBD protein (Sino Biological Inc., Beijing, China) as described previously [66]. Briefly, the scFv phage-display libraries (~10^{11} phage) were added to 3 μg of the recombinant MERS-CoV S RBD protein conjugated to 5.0 × 10^6 magnetic beads (Dynabeads M-270 epoxy, Invitrogen) and incubated with rotation for 2 h at 37 °C. The beads were washed once with 500 μL of 0.05% (*v*/*v*) Tween-20 (Sigma-Aldrich, St. Louis, MO, USA) in PBS (PBST) during the first round of biopanning. The number of washes was increased to three for the other rounds. Phages bound to beads were eluted, neutralized, allowed to infect *E. coli* ER2738 (New England Biolabs, Ipswich, MA, USA), and rescued as described previously [66].

The first randomized scFv library was subjected to two rounds of biopanning against recombinant MERS-CoV S RBD protein. The scFv phage-display library (~10^{11} phage) was added to 1.5 μg of the recombinant MERS-CoV S RBD protein conjugated to 2.5 × 10^6 magnetic beads and incubated with rotation for 2 h at 37 ℃. The beads were washed once with 500 μL of 0.5% PBST and three times with 500 μL of 0.5% PBST during the first and second rounds of biopanning, respectively. After each round of washing, bound phages were eluted and rescued as described above.

For first round of biopanning for the second and third randomized scFv libraries, the scFv phage-display libraries (~10^{11} phage) were added to 1.5 μg of the recombinant MERS-CoV S RBD protein conjugated to 2.5 × 10^6 magnetic beads and incubated

with rotation for 2 h at 37 ℃. After washing three times with 500 μL of 0.5% PBST, bound phages were eluted and rescued as described above.

Before the second round of biopanning of the second and third randomized scFv libraries, 10 μg of recombinant MERS-CoV S RBD protein was conjugated to 200 μg of non-magnetic beads (Nacalai, San Diego, CA, USA) following the manufacturer's instructions. Then, the scFv phage-display libraries (~10^{11} phage) were added to 1.5 μg of recombinant MERS-CoV S RBD protein conjugated to 2.5 × 10^6 magnetic beads and incubated on a rotator for 2 h at 37 ℃. After washing three times with 500 μL of 0.5% PBST, magnetic beads were resuspended in 100 μL of PBS and transferred to a microtube (microTUBE AFA Fiber Pre-Slit Snap-Cap, 520045, Covaris, Woburn, MA, USA) along with the recombinant MERS-COV S RBD protein-conjugated non-magnetic beads resuspended in 30 μL of PBS at a concentration of 0.33 μg/mL. Then, these bead mixtures were subjected to an ultrasound washing step using an ultrasonicator (M220, Covaris) with the following conditions: duty factor (DF) 20%, peak incident power (PIP) 12.5 W, cycles/burst 50, 20 min, and 24 ℃. After ultrasonication, magnetic beads were transferred to 1.5-mL microcentrifuge tube and washed three times with 0.5% PBST. Then, the bound phages were eluted and rescued as described above. Focused-ultrasonicator (Covaris) was used to select highly stable and aggregation-resistant clones. High shear forces were applied at the washing process to provide the required washing stringency. This approach was incorporated not only to reduce non-specific and weak-binder, but also to select the highly stable clones that can withstand high shear force. The shear force applied to the phages was adjusted not to interrupt recombinant MERS-CoV S RBD protein (Sino Biological Inc.) conjugated to magnetic beads (Invitrogen).

2.4. High-Throughput Retrieval of scFv Clones and Phage ELISA

After the fourth round of biopanning of human scFv phage-display libraries, the plasmid DNA was obtained from overnight cultures of *E. coli* cells and subjected to high-throughput retrieval of scFv clones by TrueRepertoire analysis as described previously (Celemics, Seoul, Korea) [39].

To select reactive clones to recombinant MERS-CoV S RBD protein, the scFv genes obtained from TrueRepertoire were cloned into the pComb3XSS vector [64] and used to transform *E. coli* ER2738 cells. After overnight culture, the phages were rescued from individual colonies using the M13K07 helper phage and subjected to phage ELISA as described previously [64]. Microtiter plates (Costar, Cambridge, MA, USA) were coated with 100 ng of recombinant MERS-CoV S RBD protein in coating buffer (0.1 M sodium bicarbonate, pH 8.6) at 4 ℃ overnight. The wells were blocked with 3% (*w*/*v*) bovine serum albumin (BSA; Thermo Scientific, Waltham, MA, USA) dissolved in PBS for 1 h at 37 ℃, and culture supernatant containing scFv-displayed phages that were rescued from individual colonies were added into each well. After incubation for 2 h at 37 ℃, the microtiter plates were washed three times with 0.05% PBST. Then, horseradish peroxidase (HRP)-conjugated anti-M13 monoclonal antibody (GE Healthcare) in 3% BSA/PBS was added into wells, and the plate was incubated for 1 h at 37 ℃. After washing three times with PBST, 2,2′-azino-bis-3-ethylbenzothiazoline-6-sulfonic acid solution (Thermo Scientific) was

used as the substrate for HRP. Absorbance was measured at 405 nm with a Multiskan Ascent microplate reader (Labsystems, Helsinki, Finland).

To select reactive clones from the randomized libraries, phage ELISA was performed as described previously [64] using recombinant MERS-CoV S RBD protein-coated microtiter plates. The nucleotide sequences of positive scFv clones were determined by Sanger sequencing (Cosmogenetech, Seoul, Korea).

2.5. Expression of scFv-hFc and IgG_1

The genes encoding the selected scFv clones were cloned into a modified mammalian expression vector containing the $hIgG_1$ Fc regions (hFc) at the C-terminus as described previously [67]. The expression vectors were transfected into HEK293F cells (Invitrogen), and the fusion proteins were purified by Protein A affinity chromatography as described previously [67].

For the expression of IgG_1, genes encoding V_H and V_L were amplified from the phage clones, cloned into a mammalian expression vector, and transfected into HEK293F cells. Then, IgG_1 was purified by Protein A affinity chromatography as described previously [68]. Then the eluate containing IgG_1 was subjected to gel filtration chromatography. A total of 4 mg of IgG_1 was injected at a flow rate of 1 mL/min and purified by gel filtration using a XK16/100 column packed with Superdex 200 pg at pH 7.4 (ÄKTA pure, GE Healthcare). The chromatogram was recorded at a UV absorbance of 280 nm. The fractions containing IgG_1 were pooled by collection criteria and concentrated.

2.6. ELISA

Microtiter plates (Costar) were coated with 100 ng of recombinant S glycoprotein or S RBD (wild-type, D510G, or I529T mutants; Sino Biological Inc.) in coating buffer at 4 ℃ overnight. The wells were blocked with 3% BSA/PBS for 1 h at 37 ℃. Both nebulized and non-nebulized scFv-hFc or IgG_1 were serially diluted (5-fold, 12 dilutions starting from 500 nM for scFv-hFc fusion protein or 1000 nM for IgG_1) in blocking buffer and added into individual wells. After incubation for 1 h at 37 ℃, the microtiter plates were washed three times with 0.05% PBST. Then, HRP-conjugated rabbit anti-human IgG antibody (Invitrogen) in blocking buffer (1:5000) was added into wells, and the plate was incubated for 1 h at 37 ℃. After washing three times with PBST, 2,2′-azino-bis-3-ethylbenzothiazoline-6-sulfonic acid solution (Thermo Scientific) was used as the substrate. Absorbance was measured at 405 nm using a microplate spectrophotometer (Multiskan GO; Thermo Scientific)

2.7. Nebulization

A nebulizer (Aerogen Pro, Aerogen, Galway, Ireland) was used for all experiments following the manufacturer's instructions. The nebulizer containing 1 mL of scFv-hFc fusion proteins or IgG_1 antibodies was placed on top of a 50-mL conical tube (SPL Life Sciences, Pocheon, Korea) and nebulized at a concentration of either 0.1, 0.3, or 1 mg/mL in PBS.

2.8. Microneutralization Assay

The virus (MERS-CoV/KOR/KNIH/002_05_2015, accession number KT029139.1) was obtained from the Korea National Institute of Health (kindly provided by Dr. Sung Soon Kim) and propagated in Vero cells (ATCC CCL-81) in Dulbecco's Modified Eagle's Medium (DMEM, Welgene, Gyeongsan, Republic of Korea) in the presence of 2% fetal bovine serum (Gibco). The cells were grown in T-75 flasks, inoculated with MERS-CoV, and incubated at 37 ℃ in a 5% CO_2 environment. Then 3 days after inoculation, the viruses were harvested and stored at −80 ℃. The virus titer was determined via a $TCID_{50}$ assay [69].

A neutralization assay was performed as previously described [19]. Briefly, Vero cells were seeded in 96-well plates (1×10^4 cells/well) in Opti-PRO SFM (Thermo Scientific) supplemented with 4 mM L-glutamine and 1× Antibiotics-Antimycotic (Thermo Scientific) and grown for 24 h at 37 ℃ in a 5% CO_2 environment. Two-fold serially diluted scFv-hFc fusion proteins were mixed with 100 $TCID_{50}$ of MERS-CoV, and the mixture was incubated for 30 min at 37 ℃. Then, the mixture was added to the Vero cells in tetrad and incubated for 4 days at 37 ℃ in a 5% CO_2 environment. The cytopathic effect (CPE) in each well was visualized following crystal violet staining 4 days post-infection. The IC_{50} values were calculated using the dose-response inhibition equation of GraphPad Prism 6 (GraphPad Software, La Jolla, CA, USA).

2.9. Flow Cytometry

The scFv-hFc fusion proteins (2000, 1000, 250, or 200 nM) or IgG_1 were incubated either with the recombinant S glycoprotein (200 nM) or S RBD mutants (2000 nM) fused with a polyhistidine tag at the C-terminus (Sino Biological Inc.) or without S protein in 50 μL of 1% (*w*/*v*) BSA in PBS containing 0.02% (*w*/*v*) sodium azide (FACS buffer) at 37 ℃ for 1 h. The m336 scFv-hFc and irrelevant scFv-hFc fusion proteins were used as positive and negative controls, respectively. Huh-7 cells ($hDPP4^+$) were added into v-bottom 96-well plates (Corning, Corning, NY, USA) at a density of 3×10^5 cells per well, and then, the mixture was added to the wells. After incubation at 37 ℃ for 1 h, cells were washed three times with FACS buffer and incubated with FITC-labeled rabbit anti-HIS Ab (Abcam, Cambridge, UK) at 37 ℃ for 1 h. Then, the cells were washed three times with FACS buffer, resuspended in 200 μL of PBS, and subjected to analysis by flow cytometry using a FACS Canto II instrument (BD Bioscience, San Jose, CA, USA). For each sample, 10,000 cells were assessed, and the data were analyzed using the FlowJo software (TreeStar, Ashland, OR, USA).

2.10. SE-HPLC

Non-nebulized and nebulized samples were analyzed using Waters e2695 HPLC system (Waters Corporation, Milford, MA, USA) equipped with a BioSuite high-resolution size-exclusion chromatography column (250 Å 7.5 mm × 300 mm). Each

sample (10 μg) was injected at a flow rate of 1 mL/min. The mobile phase was PBS (pH 7.4), and UV detection was performed at 280 nm/220 nm. The sample tray and column holder were maintained at 4 and 30 ℃, respectively, throughout data acquisition. The molecular weights corresponding to the antibody peaks were calculated using the Empower software (Waters Corporation).

2.11. DLS Assay

DLS experiments were performed using a Zetasizer Nano S (Malvern Panalytical Ltd., Malvern, UK) and a 633-nm/4-mW laser at a 173 ° detection angle as described previously [37]. Non-nebulized and nebulized samples were analyzed by performing three acquisitions per sample. PBS (pH 7.4) was used as the reference solvent. The results were evaluated with the Zetasizer software 7.02 (Malvern Panalytical Ltd.).

2.12. PRNT Assay

Vero cells were seeded in 12-well plates (3.5×10^5 cells/well) in Opti-PRO SFM supplemented with 4 mM L-glutamine and 1× Antibiotics-Antimycotic (Thermo Scientific) and grown for 24 h at 37 ℃ in a 5% CO_2 environment. IgG_1 antibodies were serially diluted three-fold in Dulbecco's PBS (Welgene) and mixed with an equal volume of culture media containing MERS-CoV/KOR/KNIH/002_05_2015 (100 pfu). After incubation for 1 h at 37 ℃ in a 5% CO_2 environment, the virus-antibody mixture was added to the cells and maintained for 1 h at room temperature.

The mixture was then removed, and the cells were overlaid with 1% agarose in DMEM. After incubation for 2 days at 37 ℃ in a 5% CO_2 environment, the cells were washed with PBS and fixed for 24 h with 4% paraformaldehyde. The agarose overlay was removed, and the cell monolayer was gently washed with water to remove residual agarose. The cells were stained with 0.5% crystal violet solution, and the plaques were counted manually. The number of plaques was plotted as a function of IgG_1 antibodies, and the concentration of IgG_1 at which the number of plaques was reduced by 50% compared to that in the absence of IgG_1 ($PRNT_{50}$) was calculated using GraphPad Prism 6.

2.13. HDX-MS

Deuterium oxide was acquired from Cambridge Isotope Laboratories (Tewksbury, MA, USA). Recombinant MERS-CoV S RBD protein was deglycosylated by PNGase-F (Waters Corporation) and diluted to 40 pmole in a buffer composed of 10mM potassium phosphate (pH 7.0). Hydrogen/deuterium exchange was performed by mixing 2.5 μL of recombinant MERS-CoV S RBD protein with 37.5 μL of D_2O buffer (10 mM potassium phosphate pD 7.0) and incubated for 0, 0.33 min (20 sec), 10 min, 60 min and 240 min on ice. The incubation was ended by adding 40 μL of ice-cold quench buffer (1 M TCEP, 2 M Urea, pH 2.66). The quenched samples were quickly thawed and digested by treating pepsin (Sigma-Aldrich) enzyme for 5 min on ice. Rapidly, pepsin treated samples were injected into nanoACQUITY with HDX Technology (Waters Corporation) and online-digested by passing through an Enzymate pepsin column (2.1 mm x 30 mm, 300Å, 5 μm, Waters Corporation).

Peptide fragments were subsequently trapped and desalted in VanGuard BEH C18 trap column (2.1 mm x 5 mm, 1.7 µm, Waters Corporation) at a flow rate of 100 µL/min 5% acetonitrile (ACN, Sigma-Aldrich) for 3 min and then separated by C18 analytical column (1.0 x 100 mm, 1.7 µm, Waters Corporation) at a flow rate of 40 µL/min with gradient for 13 min (started with 5% B for 1 min and increased to 40% B for 7 min). The mobile phase A was 0.1% formic acid (Sigma-Aldrich) in H_2O, and B was ACN containing 0.1 % formic acid. To minimize the back-exchange of deuterium to hydrogen, the sample, solvents, trap and analytical columns were all maintained at pH of 2.66 and 0 ℃ during analysis. Mass spectrometric analyses was performed with a SYNAPT G2-Si (Waters Corporation) equipped with Ion Mobility Separation (IMS, Waters Corporation) and standard ESI source. The mass spectra were acquired in the range of m/z 50–2000 in the positive ion mode for 10.5 min.

2.14. Peptide Identification and HDX Data Processing

Peptides were identified using the ProteinLynx Global Server 3.0.1 (PLGS, Waters Corporation) in non-deuterated samples. The following parameters were applied: monoisotopic mass, 1 missed cleavage, automatic fragment mass tolerance, and automatic peptide mass tolerance. Also, searches were performed with the variable methionine oxidation modification. To process HDX-MS data, the amount of deuterium in each peptide was determined by measuring the centroid of the isotopic distribution using DynamX 3.0 (Waters Corporation).

3. Results

3.1. Generation of Antibodies Reactive to Recombinant MERS-CoV RBD Protein From Patients

We generated human single-chain variable fragment (scFv) phage-display libraries using peripheral blood mononuclear cells (PBMCs) isolated from two MERS-CoV-infected convalescent patients. One patient (P014) was considered to be the super spreader, and the other patient (P002) was the wife of the index patient in the previous report [38]. The complexity of the libraries exceeded 3.6×10^9 and 1.9×10^9 colony-forming units for patients P002 and P014, respectively. After the third and fourth rounds of biopanning against recombinant MERS-CoV S RBD protein, the scFv clones were retrieved in a high-throughput manner as described previously [39]. Briefly, 1800 microcolonies formed on the TR chip, and of these, 542 clones with unique V_H and V_K/V_λ were identified. In these clones, 44 unique HCDR3 sequences were identified. We selected 44 clones encoding unique HCDR3 sequences and rescued phages for phage enzyme-linked immunosorbent assay (ELISA) analysis. A total of 36 unique scFv clones were highly reactive to recombinant MERS-CoV S RBD protein (Figure 1). These clones were prepared as scFv fused with human Fc (scFv-hFc) using a eukaryotic expression vector and HEK293F cells. A human anti-MERS-CoV neutralizing mAb reported previously, m336, was also prepared in this same form for use as a positive control [40].

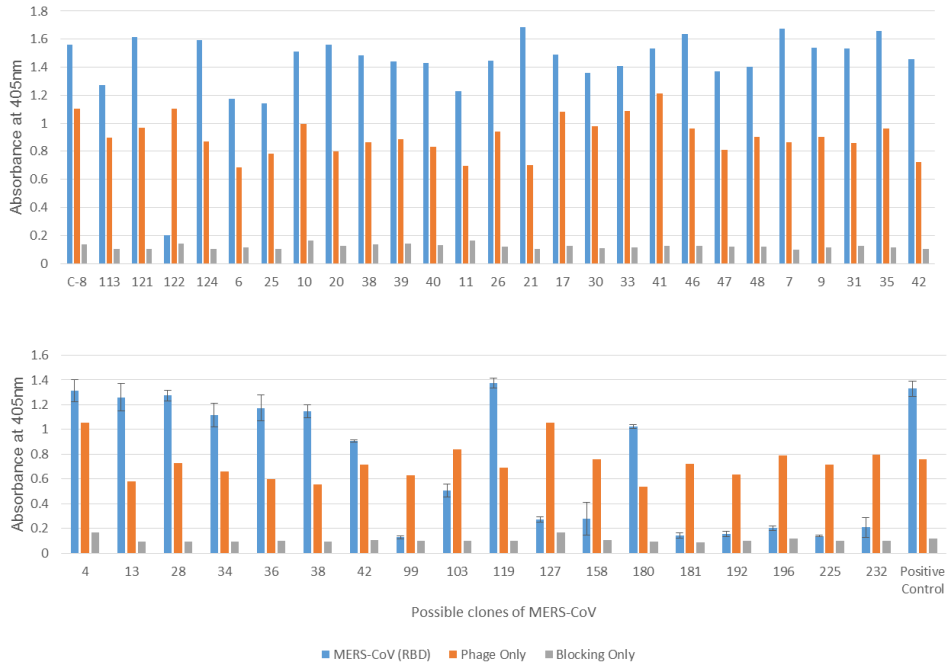

Figure 1. Reactivity of scFv clones against recombinant MERS-CoV S RBD protein

44 scFv clones encoding unique HCDR3 sequences were selected for phage ELISA analysis. scFv displaying phage clones were allowed to react with recombinant MERS-CoV S RBD protein-coated microtiter plates. The amount of bound phage was determined using HRP-conjugated anti-M13 antibody and ABTS.

3.2. Selection of MERS-CoV Neutralizing Antibodies

We performed a microneutralization assay to test the neutralizing activity of the 36 identified scFv clones against MERS-CoV (MERS-CoV/KOR/KNIH/002_05_2015). Among these, scFv clones 10, 15, 20, C-8, 34, 42, 46, 47, and 48 potently inhibited MERS-CoV replication, with half-maximal inhibitory concentration (IC_{50}) values ranging from 2.40 to 9.61 μg/mL (Figure 2 and Table 3).

Next, we tested the stability of these clones during nebulization. We nebulized the fusion proteins at a concentration of 100 μg/mL in phosphate-buffered saline (PBS) using a vibrating mesh nebulizer and then collected the aerosol. All the collected samples showed clearly visible aggregation. After centrifugation to remove the aggregated material, we repeated the ELISA analysis and compared the reactivity of pre- and post-nebulized scFv-hFc. All nine clones showed significantly reduced reactivity against recombinant S glycoprotein after nebulization (Figure 3).

We selected the clones C-8 and 48, as these antibodies exhibited the lowest IC_{50} values among the antibodies derived from patients P002 and P014, respectively. Before performing further studies, we studied the mechanism underlying inhibition of viral infection on cells. The antibodies were mixed with recombinant S glycoprotein and added to hDPP4-expressing Huh-7 cells. Both C-8 and 48 scFv-hFc nearly completely blocked binding of recombinant S glycoprotein to cells at equimolar concentration of 100 nM (Figure 4), indicating that the antibodies block the initial interaction of the virus with cells.

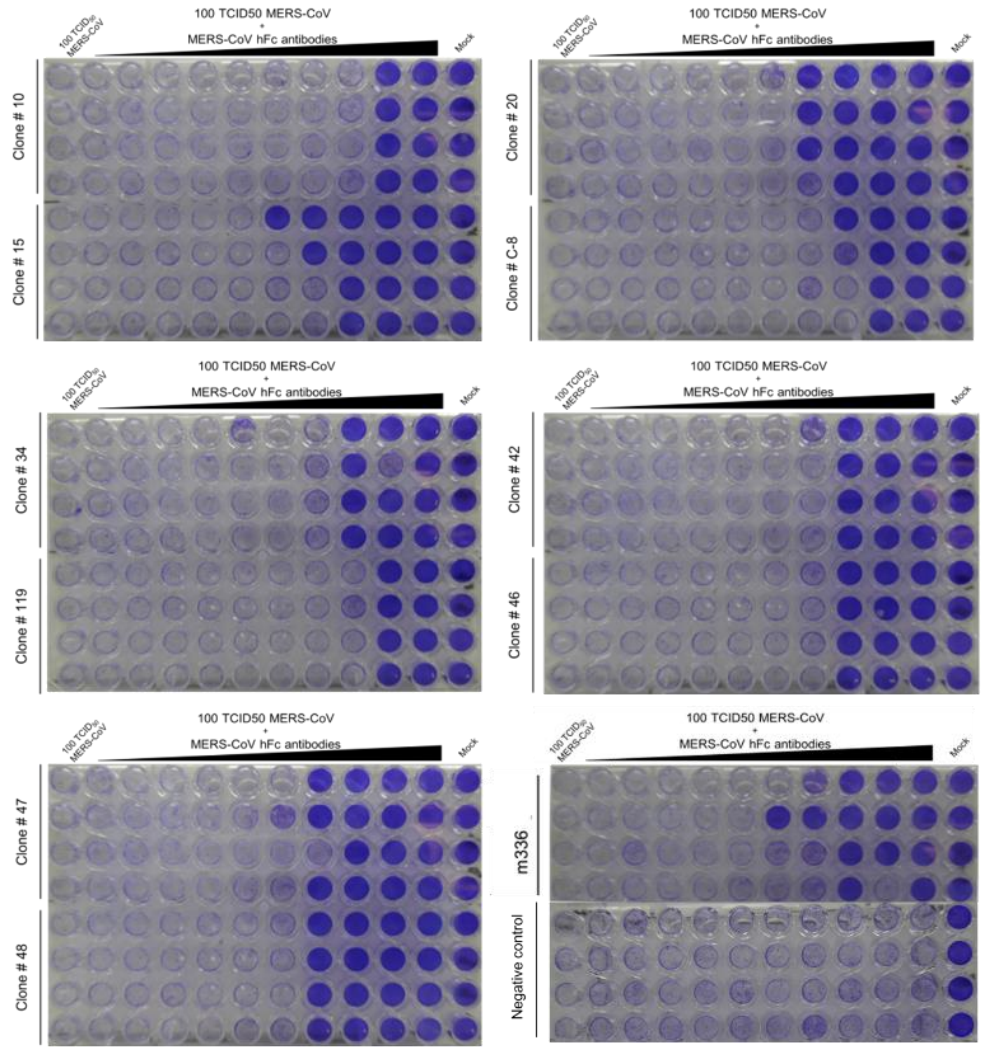

Figure 2. Effects of MERS-CoV in cytopathic effect inhibition assays of neutralizing antibodies.

Infection of Vero cells with 100 $TCID_{50}$ of MERS-CoV (strain MERS-CoV/KOR/KNIH/002_05_2015) in the presence of two-fold serially diluted (from 25 μg/ml) scFv-hFc fusion protein. After incubation, the mixture was added to Vero cells in tetrad and incubated for 4 days. CPE was visualized by crystal violet staining. The mean IC_{50} values were calculated using the dose-response inhibition equation with GraphPad Prism 6.

Table 3. Cytopathic effect inhibition by scFv clones

Clone	IC_{50} (µg/mL)
C-8	6.45
10	9.61
15	2.78
20	3.22
34	4.43
119	9.61
42	4.67
46	4.67
47	3.03
48	2.40
m336	3.71

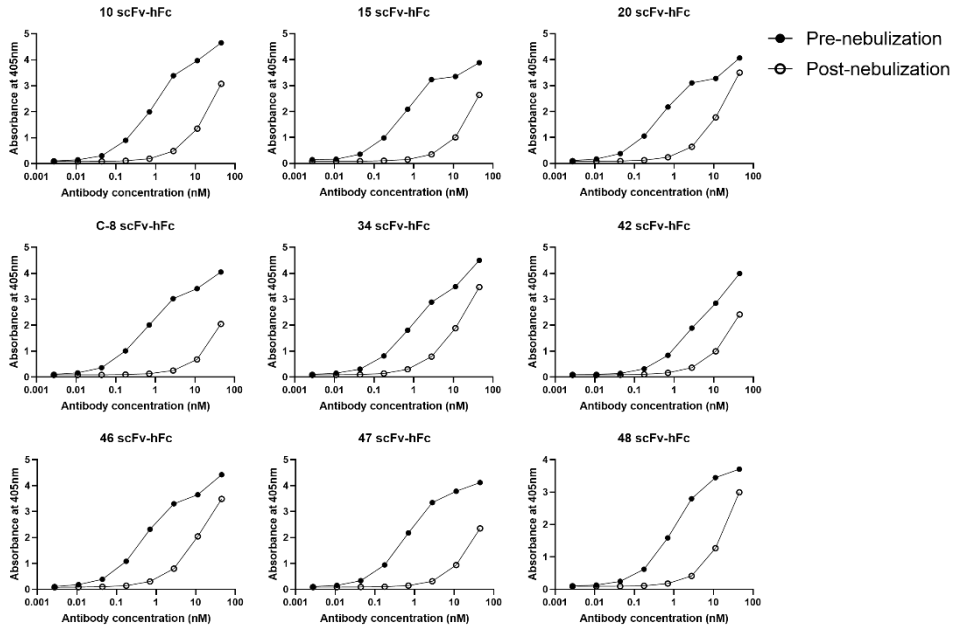

Figure 3. Reactivity of scFv clones before and after nebulization.

The scFv-hFc fusion protein was nebulized at a concentration of 100 μg/mL, and aerosol was collected. After removing aggregated material by centrifugation, the supernatant and pre-nebulized scFv-hFc fusion proteins were subjected to ELISA using recombinant S glycoprotein-coated microtiter plates. The amount of bound scFv-hFc fusion protein was determined using HRP-conjugated anti-human IgG antibody and ABTS.

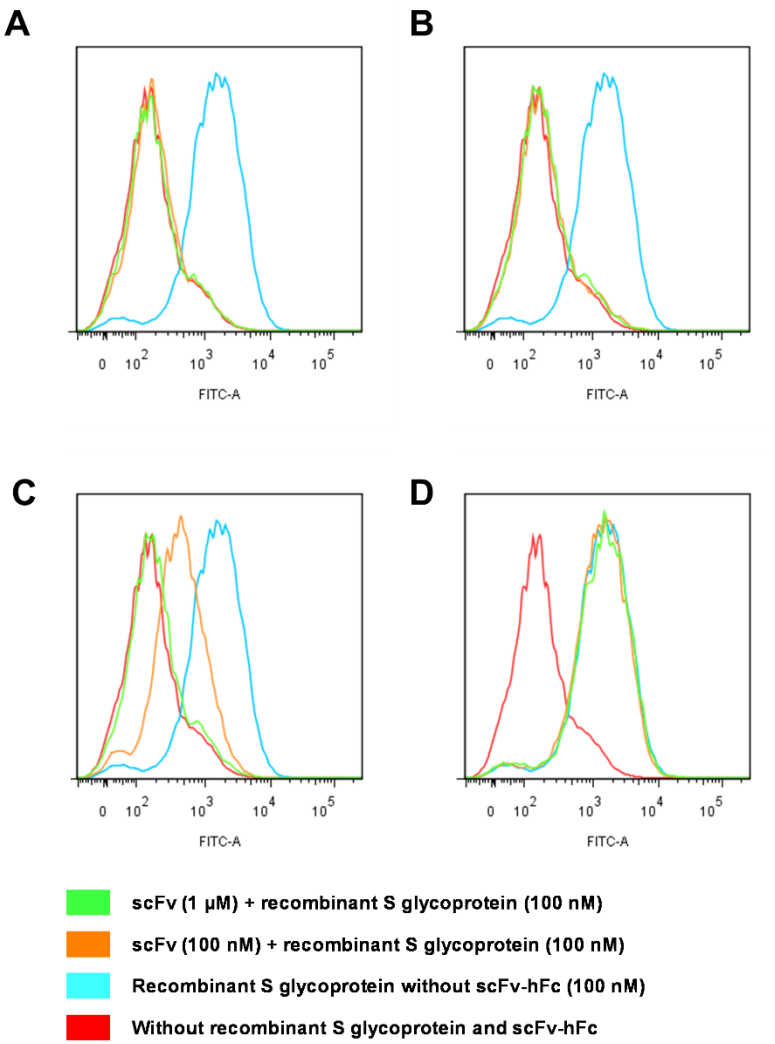

Figure 4. Flow cytometry analysis of the inhibition of recombinant S glycoprotein binding to hDPP4-expressing cells.

C-8 (A), 48 (B), m336 (C), or negative control (D) scFv-hFc were mixed and incubated with recombinant S glycoprotein fused with a polyhistidine tag at the C-terminus. After incubation with Huh-7 (hDPP4+) cells, the relative amount of bound recombinant S glycoprotein was measured using FITC-conjugated anti-HIS antibody. Per each sample, 10,000 cells were monitored, and the data were analyzed using FlowJo software.

3.3. Modification of CDR Residues to Enhance Antibody Stability

To enhance the stability of the C-8 and 48 clones, we sought to introduce mutations in CDRs, except for heavy chain CDR3 (HCDR3), for replacement of hydrophobic residues with hydrophilic residues. We defined CDRs according to the International Immunogenetics Information System (IMGT) and targeted Phe, Ile, Leu, Val, Met, Trp, and Tyr which were defined as hydrophobic amino acids in previous reports [41,42]. For the C-8 clone, the F29, Y32, I51, I52, F53, and F54 hydrophobic residues in HCDR1 and HCDR2 were selected for randomization (Figure 5A). These six residues were designed to encode the wild-type amino acid, Asp, Glu, or redundant amino acids depending on the degenerate codon in the first scFv phage-display library (Table 2). We preferred negatively charged amino acids to positively charged amino acids as lowering the isoelectric point of an antibody may reduce the non-specific *in vivo* clearance [43]. The randomized scFv phage-display library had a complexity of 2.6×10^9 colony-forming units, which exceeded the theoretical complexity of 1.3×10^5 on the nucleotide level. After two rounds of biopanning on recombinant MERS-CoV S RBD protein, we randomly rescued phage clones and performed phage ELISA. Eleven scFv clones showed reactivity to recombinant MERS-CoV S RBD protein similar to or higher than that of the original C-8 clone. The C-8-2 clone harbored F29E and Y32E replacements, while the other ten clones had only one residue replaced with either Asp, Glu, or redundant amino acids, depending on the degenerate codon. To test the stability of the C-8-2 clone during

nebulization, a scFv-hFc fusion protein was prepared and subjected to ELISA following nebulization. The reactivity of C-8-2 scFv-hFc to recombinant S glycoprotein was much less affected by nebulization than that of C-8 scFv-hFc; however, the reactivity of the C-8-2 clone was somewhat reduced compared with that of the C-8 clone (Figure 6A).

In a parallel experiment using clone 48, we prepared a randomized scFv phage-display library and selected seven clones. None of the clones were successfully expressed in the scFv-hFc format (less than 300 μg/L), preventing us from conducting further studies on clone 48.

To achieve further stabilization and affinity maturation, we generated a second scFv phage-display library using the same strategy to randomize nine residues in HCDR1 and HCDR2 of the C-8-2 clone to introduce more negatively charged residues (Figure 5A, Table 2). The proline at H52A was excluded from the randomization, as proline frequently forms a unique structure essential for antibody reactivity [44]. The second randomized scFv phage-display library had a complexity of 1.0×10^9 colony-forming units, which exceeded the theoretical complexity of 4.2×10^6 on the nucleotide level. After the second round of biopanning on recombinant MERS-CoV S RBD protein, we selected 12 clones that displayed greater reactivity to recombinant MERS-CoV S RBD protein than the C-8-2 clone in phage ELISA analysis. Clone C-8-2-4B contained replacement at six residues (G26D, T28K, S30K, S31R, G55D, and T56K; Figure 5A) and showed the highest intrinsic solubility score [45] among the 12 tested clones. Interestingly, only two residues were replaced with Asp, and four residues were replaced with positively charged amino acids, as allowed by the degenerate codons (Figure 5A). We then prepared a C-8-2-4B scFv-

hFc fusion protein using a eukaryotic expression system. After nebulization, the reactivity of C-8-2-4B scFv-hFc to recombinant S glycoprotein was less affected than either C-8 or C-8-2 scFv-hFc (Figure 6A, B). In addition, the reactivity of C-8-2-4B scFv-hFc was enhanced compared to that of C-8-2 scFv-hFc and comparable to that of C-8 scFv-hFc.

Next, we prepared C-8 and C-8-2-4B IgG_1 using a eukaryotic expression system and compared the reactivity of these immunoglobulins to recombinant S glycoprotein before and after nebulization. As expected, the reactivity of C-8-2-4B IgG_1 was better retained following nebulization than that of C-8 IgG_1 (Figure 6C). We also tested whether C-8-2-4B IgG_1 effectively blocked the interaction between recombinant S glycoprotein and hDPP4-expressing Huh-7 cells after nebulization. In flow cytometry analysis, we found that C-8-2-4B IgG_1 almost completely blocked the binding of recombinant S glycoprotein to hDPP4-expressing cells following nebulization, while C-8 IgG_1 failed to block this interaction after nebulization (Figure 6D).

As C-8-2-4B IgG_1 showed a somewhat reduced reactivity after nebulization, we sought to confer additional stability by randomizing eight hydrophobic residues in LCDRs using the same randomization scheme. We achieved 2.0×10^9 colony-forming units in the third randomized scFv phage-display library, exceeding the theoretical complexity of 2.1×10^6 (Figure 5B). After two rounds of biopanning on recombinant MERS-CoV S RBD protein, we selected clones in a phage ELISA with reactivity similar to or greater than that of C-8-2-4B. Sanger sequencing revealed that a single clone was repetitively selected. The selected clone, C-8-2-4B-10D, harbored replacements at L27C and L92V with valine (Figure 5B). We prepared C-

8-2-4B-10D IgG_1 using a eukaryotic expression system and analyzed the characteristics using ELISA, size-exclusion high-performance liquid chromatography (SE-HPLC), dynamic light scattering (DLS), and plaque reduction neutralization tests ($PRNT_{50}$). ELISA revealed a noticeable decline in reactivity to recombinant S glycoprotein by C-8 IgG_1 and m336 IgG_1 after nebulization; yet, the change in reactivity of C-8-2-4B-10D IgG_1 after nebulization was negligible (Figure 7).

In SE-HPLC analysis, high-molecular weight aggregates were detected in post-nebulization samples of C-8 and m336 IgG_1; however, no aggregate was found in post-nebulized samples of C-8-2-4B-10D IgG_1 (Table 4, Figure 8). In accordance with these SE-HPLC data, DLS analysis showed that the nebulization process converted 21.6% and 22.5% of C-8 and m336 IgG_1, respectively, into high-molecular-weight aggregates, while nebulization resulted in <1% aggregates for C-8-2-4B-10D IgG_1. (Table 4, Figure 9)

A

	HCDR1								HCDR2								Library complexity	Theoretical complexity
Kabat number	H26	H27	H28	H29	H30	H31	H32	H33	H51	H52	H52A	H53	H54	H55	H56	H57		
The first library	G	G	T	F*	S	S	Y*	A	I*	I*	P	F*	F*	G	T	A	$2.6x10^9$	$1.3x10^5$
The second library	G*	G*	T*	E	S*	S*	E	A*	I	I	P	F	F	G*	T*	A*	$1.0x10^9$	$4.2x10^6$
C-8-2-4B	D	G	K	E	K	R	E	A	I	I	P	F	F	D	K	A		

B

	LCDR1											LCDR2			LCDR3									Library complexity	Theoretical complexity
Kabat number	L27	L27A	L27B	L27C	L27D	L27E	L28	L29	L30	L31	L32	L50	L51	L52	L89	L90	L91	L92	L93	L94	L95	L96	L97		
The third library	Q	S	L*	L*	H	S	N	G	Y*	N	Y*	L*	G	S	M*	Q	A	L*	Q	T	P	L*	T	$2.0x10^9$	$2.1x10^6$
C-8-2-4B-10D	Q	S	L	V	H	S	N	G	Y	N	Y	L	G	S	M	Q	A	V	Q	T	P	L	T		

Figure 5. Sequential randomization of CDR residues of the C-8 clone.

(A) In the first randomized library, six hydrophobic amino acid residues (asterisks) in HCDR1 and HCDR2 were targeted. The second library was prepared in the C-8-2 clone by randomizing nine amino acid residues (asterisks) that were not randomized in the first randomized library. (B) Eight amino acid residues (asterisks) in LCDRs of the C-8-2-4B clone selected from the second library were randomized in the third randomized library.

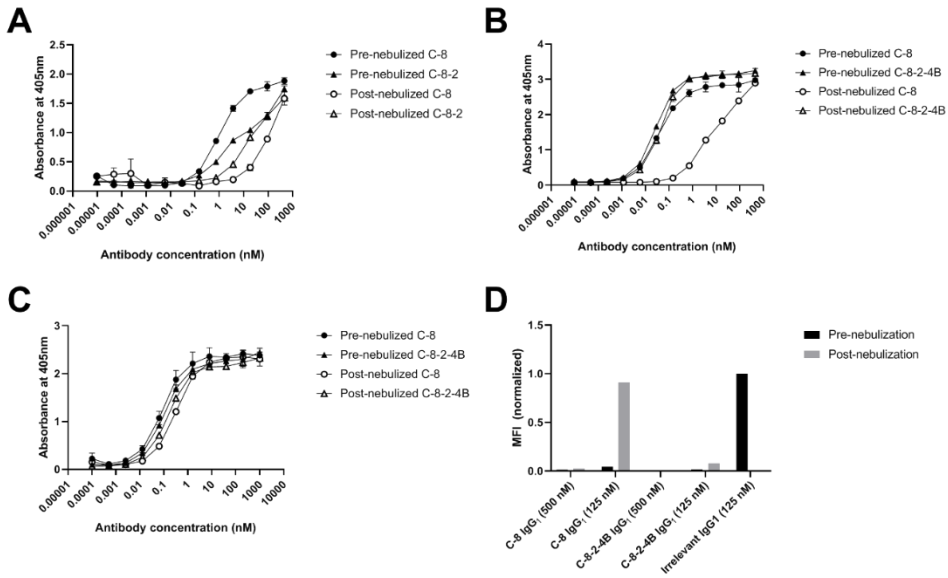

Figure 6. Biophysical characterization of C-8, C-8-2, and C-8-2-4B clones. Following nebulization at a concentration of 100 μg/mL or 300 μg/mL for scFv-hFc or IgG_1, respectively, aerosol was collected and subjected to ELISA (A–C) and flow cytometry (D). C-8-2 scFv-hFc (A), C-8-2-4B scFv-hFc (B), and C-8-2-4B IgG_1 (C) were serially diluted and incubated with recombinant S glycoprotein-coated microtiter plates. (D) C-8 IgG1 and C-8-2-4B IgG1 were incubated with recombinant S glycoprotein fused with a polyhistidine tag at the C-terminus, and the complex was allowed to react with hDPP4-expressing cells. The amount of bound recombinant S glycoprotein was measured using FITC-conjugated anti-HIS antibody. Data are representative of 10,000 cells for each sample.

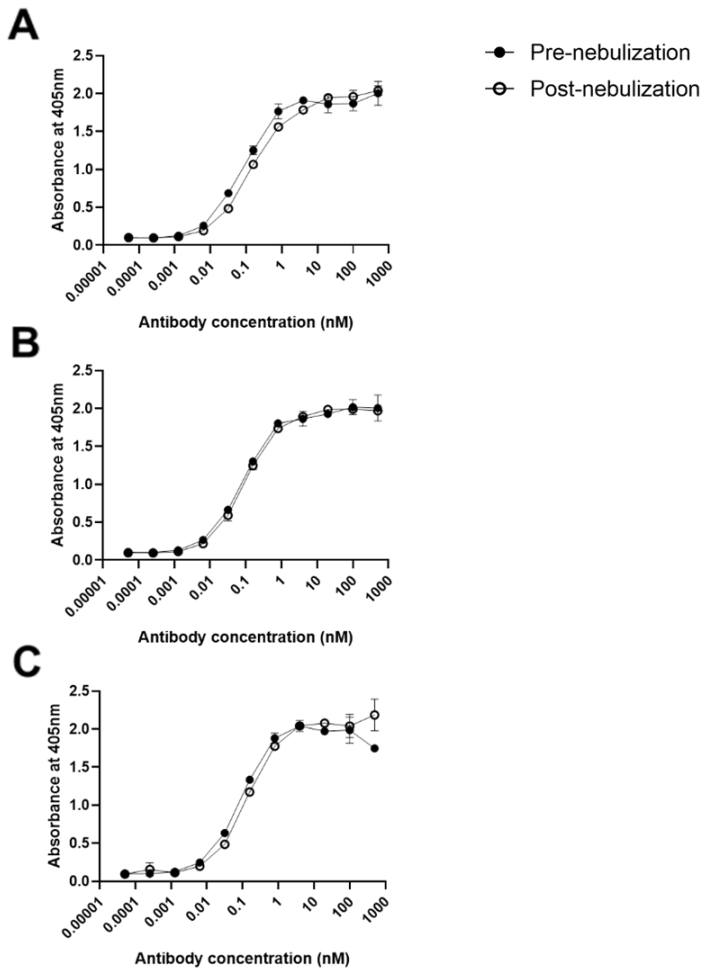

Figure 7. Reactivity of anti-MERS-CoV IgG_1 antibodies before and after nebulization.

Following nebulization at a concentration of 1 mg/mL, aerosol was collected and subjected to ELISA. Recombinant S glycoprotein-coated microtiter plates were incubated with pre-nebulized and post-nebulized C-8 IgG_1 (A), C-8-2-4B-10D IgG_1 (B), and m336 (C). HRP-conjugated anti-human IgG antibody was used as the probe, and ABTS was used as the substrate. All experiments were performed in duplicate, and the data indicate mean ± SD.

Table 4. Size-exclusion high-performance liquid chromatography (SE-HPLC) and dynamic light scattering (DLS) analysis

Antibody	SE-HPLC (% Monomer/% Aggregates)		DLS (% Monomer ± SD/% Aggregates ± SD)	
	Pre-Nebulization	Post-Nebulization	Pre-Nebulization	Post-Nebulization
C-8	100.0/0	97.9/2.1	100.0 ± 0/0	78.4 ± 3.5/21.6 ± 3.5
C-8-2-4B-10D	100.0/0	100.0/0	99.2 ± 0.7/0.8 ± 0.7	98.6 ± 0.4/1.4 ± 0.4
m336	100.0/0	99.4/0.6	96.6 ± 0.6/3.4 ± 0.6	77.5 ± 2.3/22.5 ± 2.3

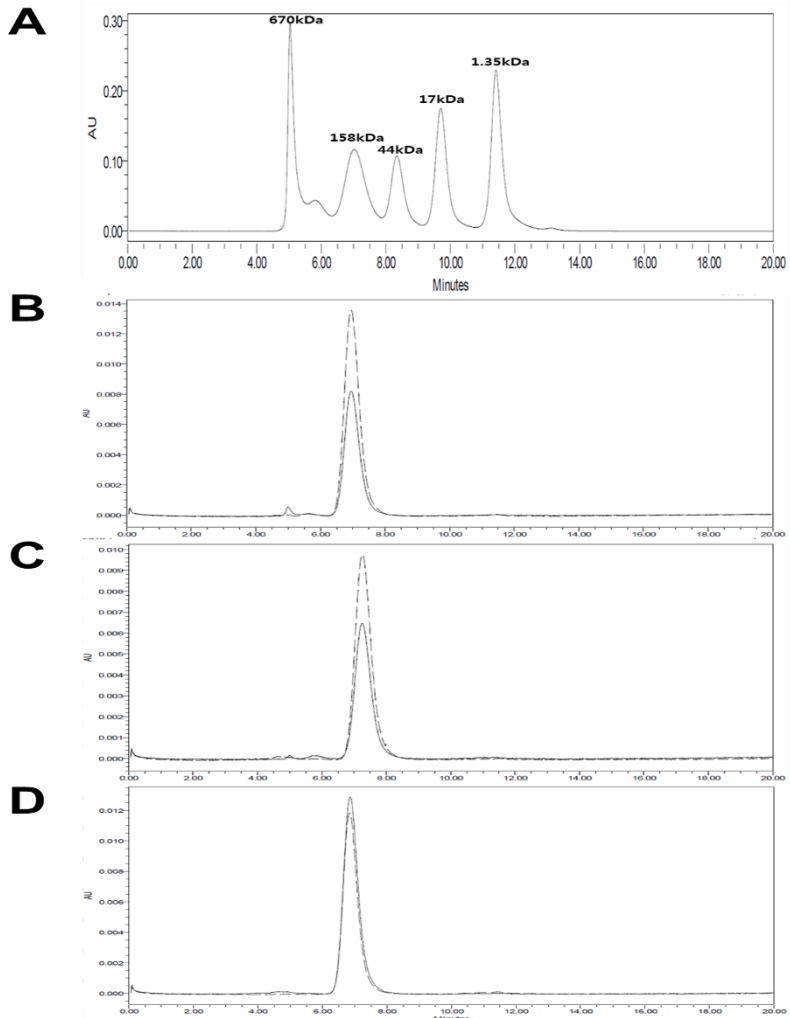

Figure 8. Size-exclusion chromatography of MERS-CoV IgG_1 antibody before and after nebulization.

Pre-nebulized (dotted lines) and post-nebulized (solid lines) samples were analyzed using Waters e2695 HPLC system. Standard (A), C-8 IgG_1 (B) m336 IgG_1 (C), and C-8-2-4B-10D IgG_1 (D) were injected at a flow rate of 1 mL/min. The mobile phase was PBS (pH 7.4), and UV detection was performed at 280 nm. The molecular weights corresponding to the antibody peaks were calculated with Empower software.

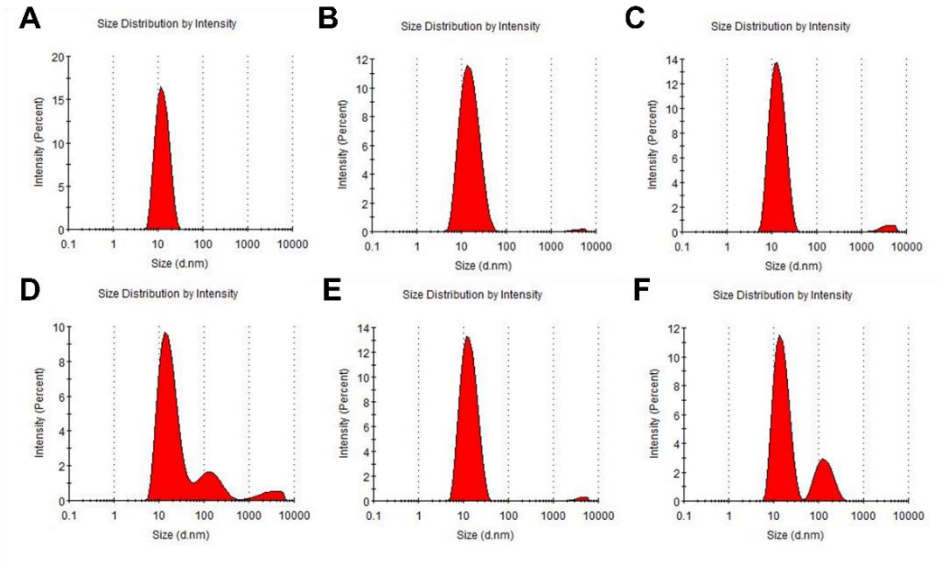

Figure 9. Dynamic light scattering analysis.

To evaluate the size distribution profile of pre-nebulized C-8 (A), pre-nebulized C-8-2-4B-10D (B), pre-nebulized m336 (C), post-nebulized C-8 (D), post-nebulized C-8-2-4B-10D (E), and post-nebulized m336 IgG_1 (F) antibodies, DLS was performed using 633-nm/4-mW laser at a 173 ° detection angle. PBS was used as the reference solvent, and the results were evaluated with Zetasizer software 7.02. All experiments were performed in triplicate, and representative results are shown for each antibody.

3.4. Neutralizing Potency After Nebulization

The neutralizing activities of pre- and post-nebulized C-8 and C-8-2-4B-10D IgG_1 were evaluated in $PRNT_{50}$ using the live MERS-CoV (MERS-CoV/KOR/KNIH/002_05_2015). Antibodies were mixed with live MERS-CoV, and then the antibody-virus mixture was allowed to infect Vero cells. C-8 and C-8-2-4B-10D IgG_1 exhibited effective inhibitory activity against MERS-CoV, with IC_{50} values of 0.29 and 0.28 μg/mL, respectively. After nebulization, C-8-2-4B-10D showed an IC_{50} value similar to that of pre-nebulized IgG_1, but the IC_{50} value of C-8 was dramatically increased following nebulization (Figure 10).

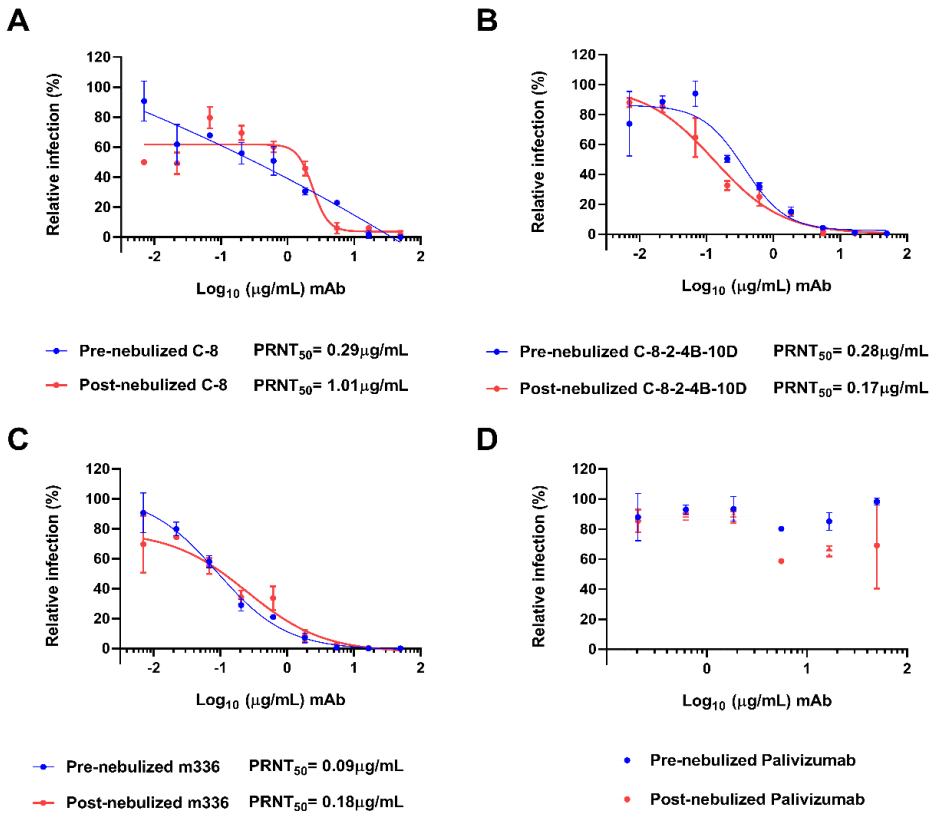

Figure 10. Neutralization of MERS-CoV by pre- and post-nebulized IgG_1.

Culture media containing 100 PFU MERS-CoV was mixed with equal volume of serially diluted C-8 IgG_1 (A), C-8-2-4B-10D IgG_1 (B), m336 IgG_1 (C), and palivizumab (D). After incubation for 1 h, the mixture was added to Vero cells. After 2 days, the plaques were counted. The inhibition of virus infection was plotted as a function of IgG_1 antibody concentration, and $PRNT_{50}$ values were calculated by GraphPad Prism 6. All experiments were performed in quadruplicate, and the data indicate mean ± SD.

3.5. Antibody binding to S protein mutants D510G, I529T, and D510G & I529T

Several polymorphisms within S protein (D510G and I529T) were identified during the MERS outbreak in South Korea. We tested binding activity of C-8 and C-8-2-4B-10D antibodies against recombinant wild-type or mutant MERS-CoV RBDs (D510G, I529T, and D510 & I529T) using ELISA analysis. ELISA revealed that the original C-8 as well as CDR-modified C-8-2-4B-10D successfully bound to recombinant MERS-CoV S RBD mutants in a dose-dependent manner without any noticeable decline in reactivity compared to that of wild-type MERS-CoV RBD (Figure 11). Furthermore, we tested whether the antibody can inhibit interaction between RBD mutants and DPP4. The antibodies were mixed with recombinant mutant MERS-CoV RBD protein (D510G, I529T, or D510G/I529T) and added to hDPP4-expressing Huh-7 cells. Both C-8 and C-8-2-4B-10D IgG_1 nearly completely blocked binding of recombinant mutant MERS-CoV RBD protein (D510G and I529T) to cells at equimolar concentration of 1000 nM (Figure 12), indicating that the antibodies block the initial interaction of the virus with cells regardless of mutations (D510G and I529T) in the RBD. In case of double mutant carrying both D510G and I529T, this mutant barely bound to hDPP4-expressing Huh-7 cells which prevent us from conducting further studies.

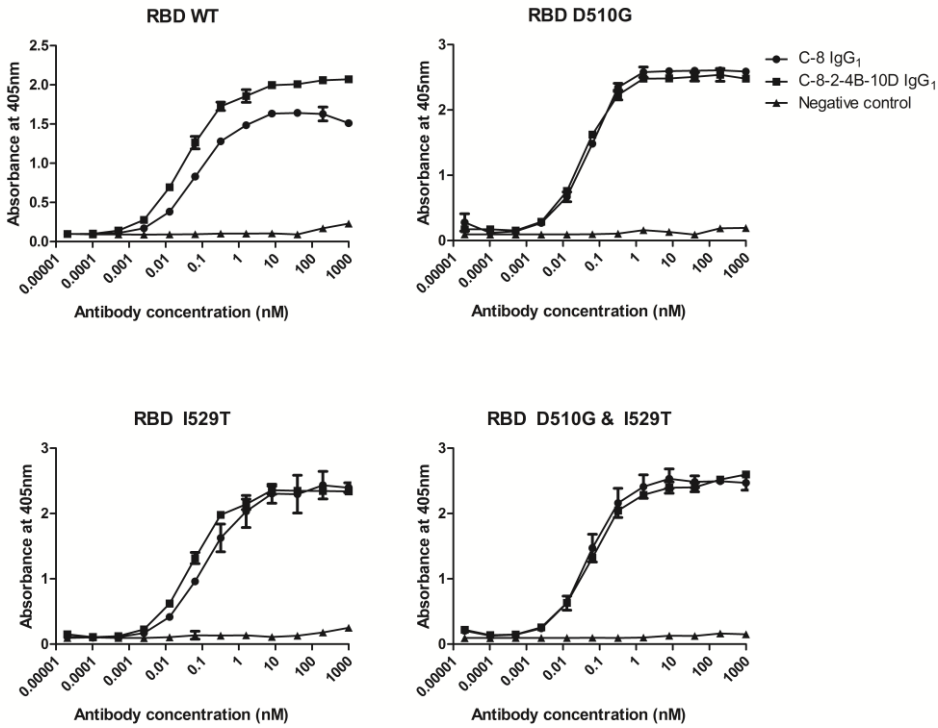

Figure 11. Reactivity of anti-MERS-CoV IgG_1 antibodies against recombinant MERS-CoV S RBD mutants.

Recombinant wild-type or mutant MERS-CoV RBD protein-coated microtiter plates were incubated with varying concentration of C-8 IgG_1, C-8-2-4B-10D IgG_1, or irrelevant IgG_1. HRP-conjugated anti-human IgG antibody was used as the probe, and ABTS was used as the substrate. All experiments were performed in duplicate, and the data indicate mean ± SD.

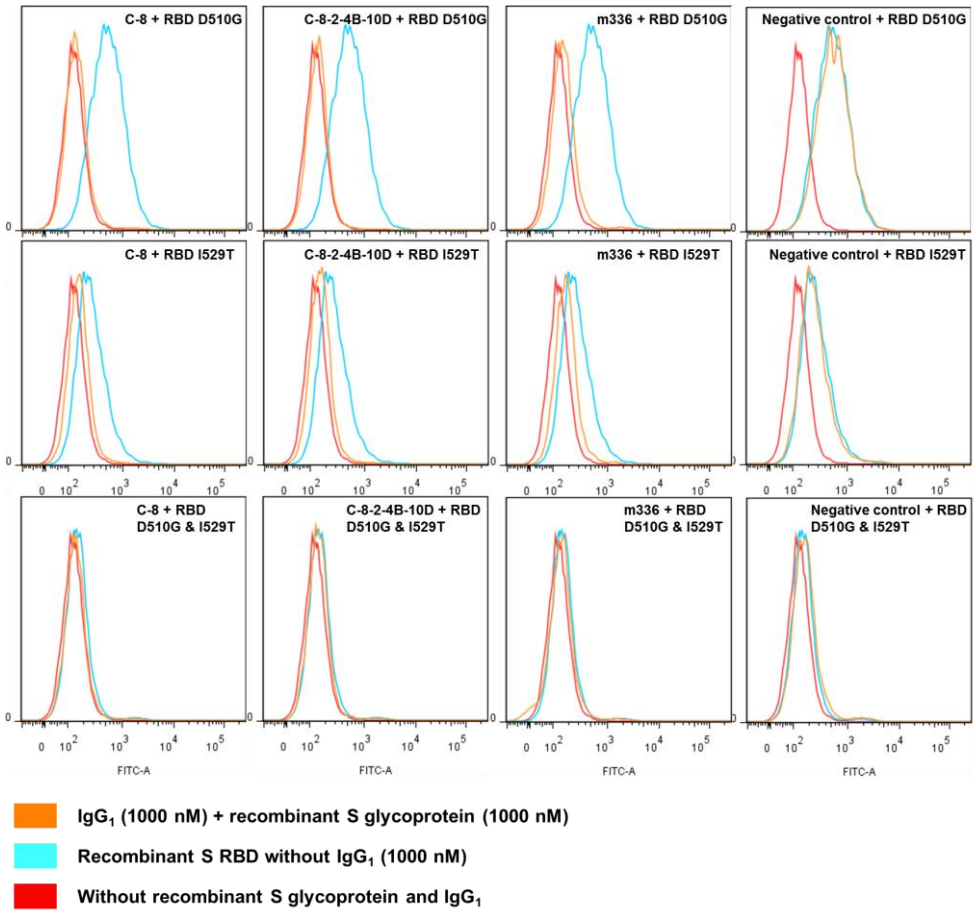

Figure 12. Flow cytometry analysis of the inhibition of recombinant mutant MERS-CoV RBD protein binding to hDPP4-expressing cells.

C-8, C-8-2-4B-10D, m336, or negative control IgG_1 were mixed and incubated with recombinant mutant MERS-CoV RBD protein fused with a polyhistidine tag at the C-terminus. After incubation with Huh-7 (hDPP4+) cells, the relative amount of bound recombinant mutant MERS-CoV RBD protein was measured using FITC-conjugated anti-HIS antibody. Per each sample, 10,000 cells were monitored, and the data were analyzed using FlowJo software.

3.6. Conformational epitope mapping by hydrogen/deuterium exchange mass spectrometry

To elucidate the site where C-8 binds, we performed hydrogen/deuterium exchange mass spectrometry (HDX-MS) and evaluated the kinetics of hydrogen/deuterium exchange at protein backbone amides. By monitoring the exchange of backbone amide hydrogen with deuterium within MERS-CoV RBD, we observed reduction in deuterium incorporation in the RBD-C-8 IgG_1 complex in residues between Ser498-Ala520 and Tyr540-Leu554 (Figure 13), indicating that these residues are involved in C-8 binding. In contrast, other regions shared almost identical deuterium levels in free and bound RBD, suggesting that these regions do not engage in protein-protein interactions. Then, we compared the C-8 epitope with the DPP4 binding site that was reported previously [16]. Surprisingly, the C-8 epitope overlapped extensively with the DPP4 binding site indicating that the C-8 block the initial interaction of the virus with natural receptor DPP4 (Figure 14).

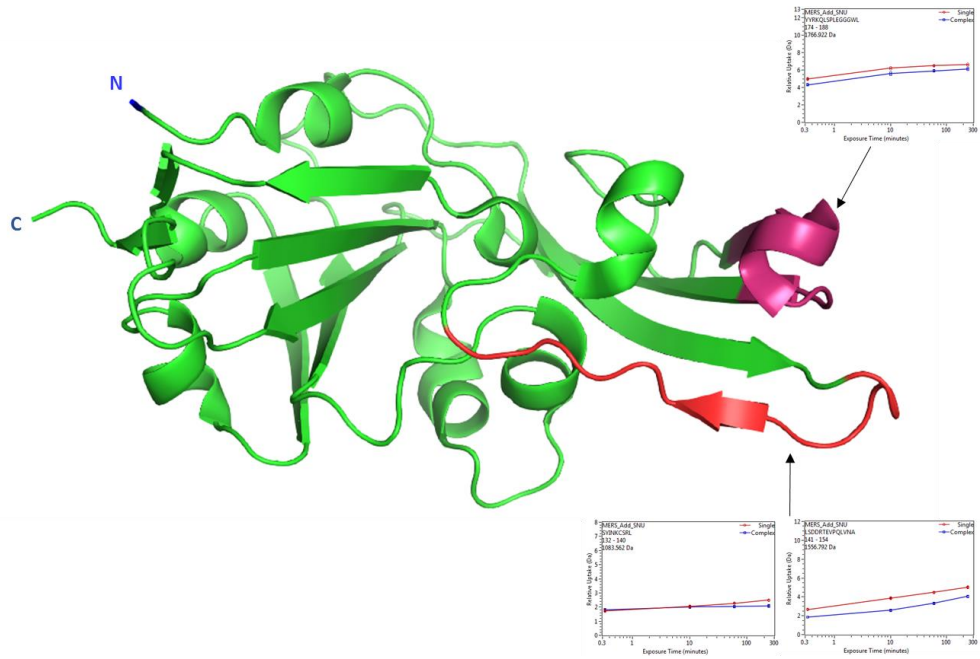

Figure 13. HDX profiles of free- and C-8 IgG_1-bound MERS-CoV RBD. The deuterium uptake graphs for peptides show the relative deuterium incorporation as a function of exposure time. The peptides that had reduction in deuterium incorporation in RBD and C-8 IgG_1 complex are highlighted in red (Ser498-Ala520) and purple (Tyr540-Leu554) on the X-ray crystal structure of MERS-CoV RBD (PDB: 4KQZ).

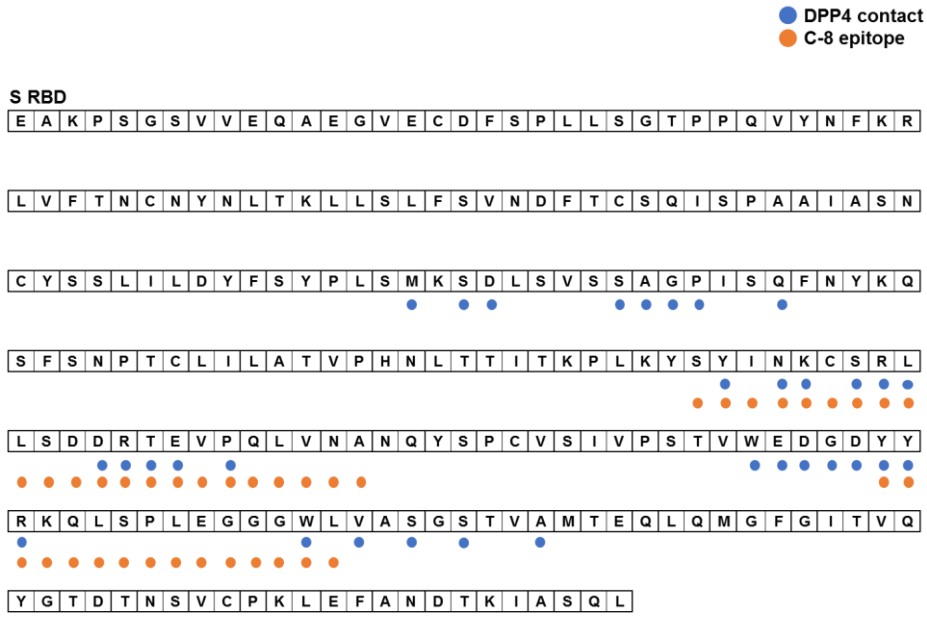

Figure 14. Mapping of the C-8 epitope and DPP4 binding site on MERS-CoV RBD sequence. RBD residues interacting with C-8 and DPP4 are marked with orange and blue dots, respectively.

4. Discussion

Pulmonary delivery can be an efficient drug delivery route to the lung parenchyma, and such delivery can sometimes exceed the efficiency of systemic injection [33]. To deliver drug via the airways, an aerosol that contains the drugs is generated by a nebulizer [46]; however, the physical stress of nebulization often causes protein instability by affecting the integrity of the molecular structure, frequently resulting in fragmentation and aggregation [47]. Aggregation of therapeutic proteins is a major concern, as it contributes to immunogenicity, which frequently causes adverse events, such as decreased drug efficacy, infusion reactions, cytokine release syndrome, or anaphylaxis [48]. A vibrating mesh nebulizer, which was designed for protein delivery, generates limited variation on the temperature, concentration, and surface tension, and its effect on the stability of the protein is the least among nebulizers [49]. This type of nebulizer also produces uniform sized particles and flow rates, which are also beneficial in maintaining the stability of biological products [37].

To reduce the immunogenicity of therapeutic protein, maintaining the stability of the native protein conformation as well as minimal (or no) formation of high-molecular weight species are crucial [50]. Therefore, engineering of a protein to render it more stable for pulmonary delivery is important. In a recent study, a trivalent nanobody against RSV F protein (ALX-O171) was successfully delivered directly into the lungs by nebulization and neutralized RSV in newborn lambs [46]. In this case, the framework 2 region of the nanobody contained more hydrophilic residues that are not observed in human V_H domains and thereby increasing the stability of the nanobody [37]. In this study, we focused on CDRs, as the sequences of the CDR loops are closely related to the folding stability of antibodies [51,52]. CDR loops

frequently possess hydrophobic residues to facilitate high binding affinity; however, solvent-exposed hydrophobic residues also impact antibody stability and aggregation [53–55]. To increase solubility and counterbalance the impact of the hydrophobic residues required for antibody binding, solubilizing residues can be introduced either at the edges of the CDR loops or within the CDR [56,57]. Furthermore, negatively charged substitution mutations within CDRs can be used to prevent aggregation [58]. In our study, we employed both strategies and reduced the number of hydrophobic residues and increased the number of charged residues in the CDRs, resulting in successful enhancement of the stability of a MERS-CoV neutralizing antibody. The final optimized antibody, C-8-2-4B-10D, showed very limited protein aggregation after nebulization and its biological potency was well maintained after such delivery. Further, we expect that formulation with surfactants such as polysorbate may prevent aggregation of this antibody during nebulization.

To test whether the C-8-2-4B-10D antibody provides better efficacy when delivered via a pulmonary route than via systemic injection, an animal model with progressive pulmonary failure is essential. In the case of hDPP4-transgenic mouse models, the infected mice exhibited central nervous system and multi-organ failure but no severe pulmonary symptoms [59–61]. Recently developed mice, which utilized CRISPR-Cas9 gene editing to modify the mouse genome to encode two amino acids (A288L and T330R) that match the human sequence in the DPP4, showed progressive pulmonary manifestations when infected with a mouse-adapted stain [25]. Following this article, we also developed the mice encoding human amino acids (288L and 330R) in the mouse DPP4; however, we were unable to generate infected mice even using the mouse-adapted strain of MERS-CoV. Thereafter, we obtained the hDPP4

knock-in mice with humanized exons 10-12 of the mouse DPP4 locus showing the progressive pulmonary manifestations when infected with a mouse-adapted strain [62]. Thus, in future studies, we will test the efficacy of C-8-2-4B-10D delivered via pulmonary route in these hDPP4-knock-in mice.

5. Reference

1. Zaki, A.M.; van Boheemen, S.; Bestebroer, T.M.; Osterhaus, A.D.; Fouchier, R.A. Isolation of a novel coronavirus from a man with pneumonia in Saudi Arabia. *N. Engl. J. Med.* **2012**, *367*, 1814–1820.

2. van Boheemen, S.; de Graaf, M.; Lauber, C.; Bestebroer, T.M.; Raj, V.S.; Zaki, A.M.; Osterhaus, A.D.; Haagmans, B.L.; Gorbalenya, A.E.; Snijder, E.J.; et al. Genomic characterization of a newly discovered coronavirus associated with acute respiratory distress syndrome in humans. *mBio* **2012**, *3*, doi:10.1128/mBio.00473-12.

3. Raj, V.S.; Mou, H.; Smits, S.L.; Dekkers, D.H.; Muller, M.A.; Dijkman, R.; Muth, D.; Demmers, J.A.; Zaki, A.; Fouchier, R.A.; et al. Dipeptidyl peptidase 4 is a functional receptor for the emerging human coronavirus-EMC. *Nature* **2013**, *495*, 251–254.

4. Consortium, F.; the, R.P.; Clst; Forrest, A.R.; Kawaji, H.; Rehli, M.; Baillie, J.K.; de Hoon, M.J.; Haberle, V.; Lassmann, T.; Kulakovskiy, I.V.; et al. A promoter-level mammalian expression atlas. *Nature* **2014**, *507*, 462–470.

5. Chan, J.F.; Choi, G.K.; Tsang, A.K.; Tee, K.M.; Lam, H.Y.; Yip, C.C.; To, K.K.; Cheng, V.C.; Yeung, M.L.; Lau, S.K.; et al. Development and Evaluation of Novel Real-Time Reverse Transcription-PCR Assays with Locked Nucleic Acid Probes Targeting Leader Sequences of Human-Pathogenic Coronaviruses. *J. Clin. Microbiol.* **2015**, *53*, 2722–2726.

6. Chan, J.F.; Lau, S.K.; Woo, P.C. The emerging novel Middle East respiratory syndrome coronavirus: The “knowns” and “unknowns”. *J. Med. Assoc.* **2013**, *112*, 372–381.

7. Oh, M.D.; Park, W.B.; Choe, P.G.; Choi, S.J.; Kim, J.I.; Chae, J.; Park, S.S.; Kim, E.C.; Oh, H.S.; Kim, E.J.; et al. Viral Load Kinetics of MERS Coronavirus Infection. *N. Engl. J. Med.* **2016**, *375*, 1303–1305.

8. Guery, B.; Poissy, J.; el Mansouf, L.; Sejourne, C.; Ettahar, N.; Lemaire, X.; Vuotto, F.; Goffard, A.; Behillil, S.; Enouf, V.; et al. Clinical features and viral diagnosis of two cases of infection with Middle East Respiratory Syndrome coronavirus: A report of nosocomial transmission. *Lancet* **2013**, *381*, 2265–2272.

9. Oh, M.D.; Park, W.B.; Park, S.W.; Choe, P.G.; Bang, J.H.; Song, K.H.; Kim, E.S.; Bin Kim, H.; Kim, N.J. Middle East respiratory syndrome: What we learned from the 2015 outbreak in the Republic of Korea. *Korean J. Intern. Med.* **2018**, *33*, 233–246.

10. Kindler, E.; Jonsdottir, H.R.; Muth, D.; Hamming, O.J.; Hartmann, R.; Rodriguez, R.; Geffers, R.; Fouchier, R.A.; Drosten, C.; Muller, M.A.; et al. Efficient replication of the novel human betacoronavirus EMC on primary human epithelium highlights its zoonotic potential. *MBio* **2013**, *4*, 11–12.

11. Zielecki, F.; Weber, M.; Eickmann, M.; Spiegelberg, L.; Zaki, A.M.; Matrosovich, M.; Becker, S.; Weber, F. Human cell tropism and innate immune system interactions of human respiratory coronavirus EMC compared to those of severe acute respiratory syndrome coronavirus. *J. Virol.* **2013**, *87*, 5300–5304.

12. Corti, D.; Misasi, J.; Mulangu, S.; Stanley, D.A.; Kanekiyo, M.; Wollen, S.; Ploquin, A.; Doria-Rose, N.A.; Staupe, R.P.; Bailey, M.; et al. Protective

monotherapy against lethal Ebola virus infection by a potently neutralizing antibody. *Science* **2016**, *351*, 1339–1342.

13. Gunn, B.M.; Yu, W.H.; Karim, M.M.; Brannan, J.M.; Herbert, A.S.; Wec, A.Z.; Halfmann, P.J.; Fusco, M.L.; Schendel, S.L.; Gangavarapu, K.; et al. A Role for Fc Function in Therapeutic Monoclonal Antibody-Mediated Protection against Ebola Virus. *Cell Host Microbe.* **2018**, *24*, 221–233.

14. Walker, L.M.; Burton, D.R. Passive immunotherapy of viral infections: 'super-antibodies' enter the fray. *Nat. Rev. Immunol.* **2018**, *18*, 297–308.

15. Du, L.; Yang, Y.; Zhou, Y.; Lu, L.; Li, F.; Jiang, S., MERS-CoV spike protein: A key target for antivirals. *Expert. Opin. Targets* **2017**, *21*, 131–143.

16. Wang, N.; Shi, X.; Jiang, L.; Zhang, S.; Wang, D.; Tong, P.; Guo, D.; Fu, L.; Cui, Y.; Liu, X.; et al. Structure of MERS-CoV spike receptor-binding domain complexed with human receptor DPP4. *Cell Res.* **2013**, *23*, 986–993.

17. Corti, D.; Zhao, J.; Pedotti, M.; Simonelli, L.; Agnihothram, S.; Fett, C.; Fernandez-Rodriguez, B.; Foglierini, M.; Agatic, G.; Vanzetta, F.; et al. Prophylactic and postexposure efficacy of a potent human monoclonal antibody against MERS coronavirus. *Proc. Natl. Acad. Sci. U. S. A.* **2015**, *112*, 10473–10478.

18. Du, L.; Zhao, G.; Yang, Y.; Qiu, H.; Wang, L.; Kou, Z.; Tao, X.; Yu, H.; Sun, S.; Tseng, C.T.; et al. A conformation-dependent neutralizing monoclonal antibody specifically targeting receptor-binding domain in Middle East respiratory syndrome coronavirus spike protein. *J. Virol.* **2014**, *88*, 7045–7053.

19. Jiang, L.; Wang, N.; Zuo, T.; Shi, X.; Poon, K.M.; Wu, Y.; Gao, F.; Li, D.; Wang, R.; Guo, J.; et al. Potent neutralization of MERS-CoV by human neutralizing monoclonal antibodies to the viral spike glycoprotein. *Sci Transl Med.* **2014**, *6*, 59.

20. Luke, T.; Wu, H.; Zhao, J.; Channappanavar, R.; Coleman, C.M.; Jiao, J.A.; Matsushita, H.; Liu, Y.; Postnikova, E.N.; Ork, B.L.; et al. Human polyclonal immunoglobulin G from transchromosomic bovines inhibits MERS-CoV in vivo. *Sci. Transl. Med.* **2016**, *8*, doi:10.1126/scitranslmed.aaf1061.

21. Pascal, K.E.; Coleman, C.M.; Mujica, A.O.; Kamat, V.; Badithe, A.; Fairhurst, J.; Hunt, C.; Strein, J.; Berrebi, A.; Sisk, J.M.; et al. Pre- and postexposure efficacy of fully human antibodies against Spike protein in a novel humanized mouse model of MERS-CoV infection. *Proc. Natl. Acad. Sci. U. S. A.* **2015**, *112*, 8738–8743.

22. Tang, X.C.; Agnihothram, S.S.; Jiao, Y.; Stanhope, J.; Graham, R.L.; Peterson, E.C.; Avnir, Y.; Tallarico, A.S.; Sheehan, J.; Zhu, Q.; et al. Identification of human neutralizing antibodies against MERS-CoV and their role in virus adaptive evolution. *Proc. Natl. Acad. Sci. U. S. A.* **2014**, *111*, 2018–2026.

23. Ying, T.; Du, L.; Ju, T.W.; Prabakaran, P.; Lau, C.C.; Lu, L.; Liu, Q.; Wang, L.; Feng, Y.; Wang, Y.; et al. Exceptionally potent neutralization of Middle East respiratory syndrome coronavirus by human monoclonal antibodies. *J. Virol.* **2014**, *88*, 7796–7805.

24. Agrawal, A.S.; Ying, T.; Tao, X.; Garron, T.; Algaissi, A.; Wang, Y.; Wang, L.; Peng, B.H.; Jiang, S.; Dimitrov, D.S.; et al. Passive Transfer of A Germline-like Neutralizing Human Monoclonal Antibody Protects Transgenic Mice Against Lethal Middle East Respiratory Syndrome Coronavirus Infection. *Sci. Rep.* **2016**, *6*, 31629.

25. Cockrell, A.S.; Yount, B.L.; Scobey, T.; Jensen, K.; Douglas, M.; Beall, A.; Tang, X.C.; Marasco, W.A.; Heise, M.T.; Baric, R.S. A mouse model for MERS

coronavirus-induced acute respiratory distress syndrome. *Nat. Microbiol.* **2016**, *2*, 16226.

26. Fan, C.; Wu, X.; Liu, Q.; Li, Q.; Liu, S.; Lu, J.; Yang, Y.; Cao, Y.; Huang, W.; Liang, C.; Ying, T.; Jiang, S.; Wang, Y., A Human DPP4-Knockin Mouse's Susceptibility to Infection by Authentic and Pseudotyped MERS-CoV. *Viruses* **2018,** 10, (9).

27. Houser, K.V.; Gretebeck, L.; Ying, T.; Wang, Y.; Vogel, L.; Lamirande, E.W.; Bock, K.W.; Moore, I.N.; Dimitrov, D.S.; Subbarao, K., Prophylaxis With a Middle East Respiratory Syndrome Coronavirus (MERS-CoV)-Specific Human Monoclonal Antibody Protects Rabbits From MERS-CoV Infection. *J. Infect. Dis.* **2016**, *213*, 1557–1561.

28. Johnson, R.F.; Bagci, U.; Keith, L.; Tang, X.; Mollura, D.J.; Zeitlin, L.; Qin, J.; Huzella, L.; Bartos, C.J.; Bohorova, N.; et al. 3B11-N, a monoclonal antibody against MERS-CoV, reduces lung pathology in rhesus monkeys following intratracheal inoculation of MERS-CoV Jordan-n3/2012. *Virology* **2016**, *490*, 49–58.

29. Li, Y.; Wan, Y.; Liu, P.; Zhao, J.; Lu, G.; Qi, J.; Wang, Q.; Lu, X.; Wu, Y.; Liu, W.; et al. A humanized neutralizing antibody against MERS-CoV targeting the receptor-binding domain of the spike protein. *Cell Res.* **2015**, *25*, 1237–1249.

30. Qiu, H.; Sun, S.; Xiao, H.; Feng, J.; Guo, Y.; Tai, W.; Wang, Y.; Du, L.; Zhao, G.; Zhou, Y. Single-dose treatment with a humanized neutralizing antibody affords full protection of a human transgenic mouse model from lethal Middle East respiratory syndrome (MERS)-coronavirus infection. *Antivir. Res.* **2016**, *132*, 141–148.

31. Hart, T.K.; Cook, R.M.; Zia-Amirhosseini, P.; Minthorn, E.; Sellers, T.S.; Maleeff, B.E.; Eustis, S.; Schwartz, L.W.; Tsui, P.; Appelbaum, E.R.; et al. Preclinical efficacy and safety of mepolizumab (SB-240563), a humanized monoclonal antibody to IL-5, in cynomolgus monkeys. *J. Allergy Clin. Immunol.* **2001**, *108*, 250–257.

32. Koleba, T.; Ensom, M.H., Pharmacokinetics of intravenous immunoglobulin: A systematic review. *Pharmacotherapy* **2006**, *26*, 813–827.

33. Guilleminault, L.; Azzopardi, N.; Arnoult, C.; Sobilo, J.; Herve, V.; Montharu, J.; Guillon, A.; Andres, C.; Herault, O.; Le Pape, A.; et al. Fate of inhaled monoclonal antibodies after the deposition of aerosolized particles in the respiratory system. *J. Control. Release* **2014**, *196*, 344–354.

34. Bitonti, A.J.; Dumont, J.A. Pulmonary administration of therapeutic proteins using an immunoglobulin transport pathway. *Adv. Drug Deliv. Rev.* **2006**, *58*, 1106–1118.

35. Bitonti, A.J.; Dumont, J.A.; Low, S.C.; Peters, R.T.; Kropp, K.E.; Palombella, V.J.; Stattel, J.M.; Lu, Y.; Tan, C.A.; Song, J.J.; et al. Pulmonary delivery of an erythropoietin Fc fusion protein in non-human primates through an immunoglobulin transport pathway. *Proc. Natl. Acad. Sci. U. S. A.* **2004**, *101*, 9763–9768.

36. Low, S.C.; Nunes, S.L.; Bitonti, A.J.; Dumont, J.A. Oral and pulmonary delivery of FSH-Fc fusion proteins via neonatal Fc receptor-mediated transcytosis. *Hum. Reprod.* **2005**, *20*, 1805–1813.

37. Van Heeke, G.; Allosery, K.; De Brabandere, V.; De Smedt, T.; Detalle, L.; de Fougerolles, A. Nanobodies(R) as inhaled biotherapeutics for lung diseases. *Pharm. Ther.* **2017**, *169*, 47–56.

38. Kim, Y.S.; Aigerim, A.; Park, U.; Kim, Y.; Rhee, J.Y.; Choi, J.P.; Park, W.B.; Park, S.W.; Kim, Y.; Lim, D.G.; et al. Sequential Emergence and Wide Spread of Neutralization Escape Middle East Respiratory Syndrome Coronavirus Mutants, South Korea, 2015. *Emerg. Infect. Dis.* **2019**, *25*, 1161–1168.

39. Noh, J.; Kim, O.; Jung, Y.; Han, H.; Kim, J.E.; Kim, S.; Lee, S.; Park, J.; Jung, R.H.; Kim, S.I.; et al. High-throughput retrieval of physical DNA for NGS-identifiable clones in phage display library. *MAbs* **2019**, *11*, 532–545.

40. Ying, T.; Prabakaran, P.; Du, L.; Shi, W.; Feng, Y.; Wang, Y.; Wang, L.; Li, W.; Jiang, S.; Dimitrov, D.S.; et al. Junctional and allele-specific residues are critical for MERS-CoV neutralization by an exceptionally potent germline-like antibody. *Nat. Commun.* **2015**, *6*, 8223.

41. Pommie, C.; Levadoux, S.; Sabatier, R.; Lefranc, G.; Lefranc, M.P. IMGT standardized criteria for statistical analysis of immunoglobulin V-REGION amino acid properties. *J. Mol. Recognit.* **2004**, *17*, 17–32.

42. Tartaglia, G.G.; Cavalli, A.; Pellarin, R.; Caflisch, A., Prediction of aggregation rate and aggregation-prone segments in polypeptide sequences. *Protein Sci.* **2005**, *14*, 2723–2734.

43. Igawa, T.; Tsunoda, H.; Tachibana, T.; Maeda, A.; Mimoto, F.; Moriyama, C.; Nanami, M.; Sekimori, Y.; Nabuchi, Y.; Aso, Y.; et al. Reduced elimination of IgG antibodies by engineering the variable region. *Protein Eng. Des. Sel.* **2010**, *23*, 385–392.

44. Feige, M.J.; Hendershot, L.M.; Buchner, J. How antibodies fold. *Trends Biochem. Sci.* **2010,** *35,* 189–198.

45. Sormanni, P.; Amery, L.; Ekizoglou, S.; Vendruscolo, M.; Popovic, B., Rapid and accurate in silico solubility screening of a monoclonal antibody library. *Sci. Rep.* **2017**, *7,* 8200.

46. Larios Mora, A.; Detalle, L.; Gallup, J.M.; Van Geelen, A.; Stohr, T.; Duprez, L.; Ackermann, M.R. Delivery of ALX-0171 by inhalation greatly reduces respiratory syncytial virus disease in newborn lambs. *MAbs* **2018**, *10*, 778–795.

47. Respaud, R.; Marchand, D.; Parent, C.; Pelat, T.; Thullier, P.; Tournamille, J.F.; Viaud-Massuard, M.C.; Diot, P.; Si-Tahar, M.; Vecellio, L.; et al. Effect of formulation on the stability and aerosol performance of a nebulized antibody. *MAbs* **2014**, *6,* 1347–1355.

48. Moussa, E.M.; Panchal, J.P.; Moorthy, B.S.; Blum, J.S.; Joubert, M.K.; Narhi, L.O.; Topp, E.M. Immunogenicity of Therapeutic Protein Aggregates. *J. Pharm. Sci.* **2016**, *105*, 417–430.

49. Beck-Broichsitter, M.; Kleimann, P.; Schmehl, T.; Betz, T.; Bakowsky, U.; Kissel, T.; Seeger, W., Impact of lyoprotectants for the stabilization of biodegradable nanoparticles on the performance of air-jet, ultrasonic, and vibrating-mesh nebulizers. *Eur. J. Pharm. Biopharm.* **2012**, *82*, 272–280.

50. Rosenberg, A.S. Effects of protein aggregates: An immunologic perspective. *AAPS J.* **2006**, *8*, 501–507.

51. Ewert, S.; Huber, T.; Honegger, A.; Pluckthun, A., Biophysical properties of human antibody variable domains. *J. Mol. Biol.* **2003**, *325*, 531–553.

52. Honegger, A.; Malebranche, A.D.; Rothlisberger, D.; Pluckthun, A. The influence of the framework core residues on the biophysical properties of immunoglobulin heavy chain variable domains. *Protein Eng. Des. Sel.* **2009**, *22*, 121–134.

53. Chennamsetty, N.; Voynov, V.; Kayser, V.; Helk, B.; Trout, B.L. Design of therapeutic proteins with enhanced stability. *Proc. Natl. Acad. Sci. U. S. A.* **2009**, *106*, 11937–11942.

54. Wang, X.; Das, T.K.; Singh, S.K.; Kumar, S. Potential aggregation prone regions in biotherapeutics: A survey of commercial monoclonal antibodies. *MAbs* **2009**, *1*, 254–267.

55. Wu, S.J.; Luo, J.; O'Neil, K.T.; Kang, J.; Lacy, E.R.; Canziani, G.; Baker, A.; Huang, M.; Tang, Q.M.; Raju, T.S.; et al. Structure-based engineering of a monoclonal antibody for improved solubility. *Protein Eng. Des. Sel.* **2010**, *23*, 643–651.

56. Jespers, L.; Schon, O.; Famm, K.; Winter, G. Aggregation-resistant domain antibodies selected on phage by heat denaturation. *Nat. Biotechnol.* **2004**, *22*, 1161–1165.

57. Perchiacca, J.M.; Bhattacharya, M.; Tessier, P.M. Mutational analysis of domain antibodies reveals aggregation hotspots within and near the complementarity determining regions. *Proteins* **2011**, *79*, 2637–2647.

58. Dudgeon, K.; Rouet, R.; Kokmeijer, I.; Schofield, P.; Stolp, J.; Langley, D.; Stock, D.; Christ, D. General strategy for the generation of human antibody variable domains with increased aggregation resistance. *Proc. Natl. Acad. Sci. U. S. A.* **2012**, *109*, 10879–10884.

59. Agrawal, A.S.; Garron, T.; Tao, X.; Peng, B.H.; Wakamiya, M.; Chan, T.S.; Couch, R.B.; Tseng, C.T. Generation of a transgenic mouse model of Middle East respiratory syndrome coronavirus infection and disease. *J. Virol.* **2015**, *89*, 3659–3670.

60. Li, K.; Wohlford-Lenane, C.; Perlman, S.; Zhao, J.; Jewell, A.K.; Reznikov, L.R.; Gibson-Corley, K.N.; Meyerholz, D.K.; McCray, P.B., Jr. Middle East Respiratory Syndrome Coronavirus Causes Multiple Organ Damage and Lethal Disease in Mice Transgenic for Human Dipeptidyl Peptidase 4. *J. Infect. Dis.* **2016**, *213*, 712–722.

61. Zhao, G.; Jiang, Y.; Qiu, H.; Gao, T.; Zeng, Y.; Guo, Y.; Yu, H.; Li, J.; Kou, Z.; Du, L.; et al. Multi-Organ Damage in Human Dipeptidyl Peptidase 4 Transgenic Mice Infected with Middle East Respiratory Syndrome-Coronavirus. *PLoS ONE* **2015**, *10*, 145561.

62. Li, K.; Wohlford-Lenane, C.L.; Channappanavar, R.; Park, J.E.; Earnest, J.T.; Bair, T.B.; Bates, A.M.; Brogden, K.A.; Flaherty, H.A.; Gallagher, T.; et al. Mouse-adapted MERS coronavirus causes lethal lung disease in human DPP4 knockin mice. *Proc. Natl. Acad. Sci. U. S. A.* **2017**, *114*, E3119–E3128.

63. Kanof, M.E.; Smith, P.D.; Zola, H. Isolation of whole mononuclear cells from peripheral blood and cord blood. *Curr. Protoc. Immunol.* **2001**, doi:10.1002/0471142735.im0701s85.

64. Carlos, F. Barbas III, Dennis, R. Burton, Jamie, K. Scott, Gregg, J. Silverman. Phage Display: A Laboratory Manual. Cold Spring Harbor Laboratory Press. **2001**. https://doi.org/10.1086/420571

65. Andris-Widhopf, J.; Steinberger, P.; Fuller, R.; Rader, C.; Barbas, C.F. 3rd, Generation of human scFv antibody libraries: PCR amplification and assembly of light- and heavy-chain coding sequences. *Cold Spring Harb. Protoc.* **2011**, *2011*, doi:10.1101/pdb.prot065565.

66. Lee, Y.; Kim, H.; Chung, J., An antibody reactive to the Gly63-Lys68 epitope of NT-proBNP exhibits O-glycosylation-independent binding. *Exp. Mol. Med.* **2014**, *46*, 114.

67. Lee, S.; Yoon, I.H.; Yoon, A.; Cook-Mills, J.M.; Park, C.G.; Chung, J. An antibody to the sixth Ig-like domain of VCAM-1 inhibits leukocyte transendothelial migration without affecting adhesion. *J. Immunol.* **2012**, *189*, 4592–4601.

68. Jin, J.; Park, G.; Park, J.B.; Kim, S.; Kim, H.; Chung, J. An anti-EGFR x cotinine bispecific antibody complexed with cotinine-conjugated duocarmycin inhibits growth of EGFR-positive cancer cells with KRAS mutations. *Exp. Mol. Med.* **2018**, *50*, 67.

69. Reed, L.J.; Muench, H., A Simple Method for Estimating Fifty Per Cent. Endpoints. *Am. J. Epidemiol.* **1938,** *27*, 493-497

초 록

사우디아라비아 환자에게서 2012년에 최초로 분리된 중동호흡기증후군 코로나바이러스 (Middle East respiratory syndrome coronavirus, MERS-CoV)는 2015년 한국에서 빠르게 확산되어 2달 동안 186명의 감염 환자와 38명의 사망자를 발생시켰다. MERS-CoV 감염 환자의 치사율은 약 35%로 상당히 높지만, 현재까지 백신 및 치료제가 전무하다. 따라서 신, 변종 바이러스의 도래로 인한 국가적 감염병 대응 기반 마련을 위해 MERS-CoV를 효율적으로 중화시키는 인간 항체의 개발이 시급한 상황이다.

MERS-Cov는 감염 환자에게 호흡기 부전을 유발 할 수 있으며, 심각한 경우 환자는 기계적 인공호흡에 의존해야 한다. 폐 질환에서 치료용 항체를 전신 투여할 경우, 극히 제한된 양의 항체만 폐에서 검출된다. 이러한 전신 투여의 한계를 보완하기 위해 분무된 항체를 흡입하는 방법이 새로운 대안으로 인식되고 있다. 그러나, 항체를 분무하는 과정에서 다양한 생리학적 스트레스가 발생하므로, 항체는 이와 같은 스트레스에 내성이 있어야 하고, 안정성이 유지되어야 하며, 최소한의 응집체를 형성해야 한다.

본 연구에서는 Spike (S) 당단백질 수용체 결합 도메인 (receptor binding domain, RBD)에 결합하는 인간 항체의 선별을 위해 중동호흡기증후군에 이환 되었다가 회복한 2명의 환자로부터 항체 라이브러리를 제조하였으며, 시험관내 시험에서 MERS-CoV의 감염을

강력히 억제하는 다수의 항체들을 선별하였다. 분무 과정에서 항체의 안정성을 높이기 위해, 항체의 상보성 결정 영역 (Complementarity determining region, CDR)에 돌연변이를 도입하였으며, 그 결과 변형 전의 클론과 비교하여 분무 후에 상당히 큰 안정성, 동등한 반응성 및 중화능을 갖는 클론을 성공적으로 생성하였다. 요약하자면, CDR에 안정화 돌연변이를 도입함으로써, 분무를 통해 폐 경로로 전달이 가능한 항 MERS-CoV 중화 인간 항체를 성공적으로 개발하였다.

주요어 : 중동호흡기증후군 코로나바이러스, 에어로졸 전달, 항체 엔지니어링, 중화 항체, 네뷸라이저 요법

학번 : 2014-25080